Atmospheric Research 102 (2011) 263–285

Contents lists available at SciVerse ScienceDirect

Atmospheric Research

journal homepage: www.elsevier.com/locate/atmos

Multiscale modeling of the moist-convective atmosphere — A review

A. Arakawa [a], J.-H. Jung [b,*]

[a] University of California, Los Angeles, CA, USA
[b] Colorado State University, Fort Collins, CO, USA

ARTICLE INFO

Article history:
Received 23 March 2011
Received in revised form 24 August 2011
Accepted 24 August 2011

Keywords:
Atmospheric modeling
Moist convection
Cumulus parameterization
Multiscale modeling
Unified parameterization
Quasi-3D multiscale modeling framework (MMF)

ABSTRACT

Multiscale modeling of the moist-convective atmosphere is reviewed with an emphasis on the recently proposed approaches of unified parameterization and Quasi-3D (Q3D) Multiscale Modeling Framework (MMF). The cumulus parameterization problem, which was introduced to represent the multiscale effects of moist convection, has been one of the central issues in atmospheric modeling. After a review of the history of cumulus parameterization, it is pointed out that currently there are two families of atmospheric models with quite different formulations of model physics, one represented by the general circulation models (GCMs) and the other by the cloud-resolving models (CRMs). Ideally, these two families of models should be unified so that a continuous transition of model physics from one kind to the other takes place as the resolution changes. This paper discusses two possible routes to achieve the unification. ROUTE I unifies the cumulus parameterization in conventional GCMs and the cloud microphysics parameterization in CRMs. A key to construct such a unified parameterization is to reformulate the vertical eddy transport due to subgrid-scale moist convection in such a way that it vanishes when the resolution is sufficiently high. A preliminary design of the unified parameterization is presented with supporting evidence for its validity. ROUTE II for the unification follows the MMF approach based on a coupled GCM/CRM, originally known as the "super-parameterization". The Q3D MMF is an attempt to broaden the applicability of the super-parameterization without necessarily using a fully three-dimensional CRM. This is accomplished using a network of cloud-resolving grids with gaps. The basic Q3D algorithm and highlights of preliminary results are reviewed. It is suggested that the hierarchy of future global models should form a "Multiscale Modeling Network (MMN)", which combines these two routes. With this network, the horizontal resolution of the dynamics core and that of the physical processes can be individually and freely chosen without changing the formulation of model physics. Development of such a network will represent a new phase of the history of numerical modeling of the atmosphere that can be characterized by the keyword "unification".

Contents

* Corresponding author at: Department of Atmospheric Science, Colorado State University, Fort Collins, Colorado 80523, USA. Tel.: +1 970 491 8591.
E-mail address: jung@atmos.colostate.edu (J.-H. Jung).

0169-8095 © 2011 Elsevier B.V. Open access under CC BY-NC-ND license.
doi:10.1016/j.atmosres.2011.08.009

1. Introduction

As illustrated in Fig. 1, clouds and their associated physical processes strongly influence the atmosphere in the following ways (Arakawa, 1975):

- By coupling dynamical and hydrological processes in the atmosphere through the heat of condensation and evaporation and through redistributions of sensible and latent heat and momentum;
- By coupling radiative and dynamical-hydrological processes in the atmosphere through the reflection, absorption, and emission of radiation;
- By influencing hydrological processes in the ground through precipitation; and
- By influencing the couplings between the atmosphere and oceans (or ground) through modifications of radiation and planetary boundary layer (PBL) processes.

It is important to note that most of these interactions are two-way interactions. For example, the amount of latent heat release through condensation is strongly coupled with the motion so that the heat of condensation is a result of the motion as well as a cause of the motion. Thus, although the release of latent heat is a dominant component of the atmosphere's sensible heat budget, it is not correct to say that the atmospheric motions are "forced" by the heat of condensation (see Emanuel et al., 1994). Similar situations exist for all of the two-way interactions shown in Fig. 1.

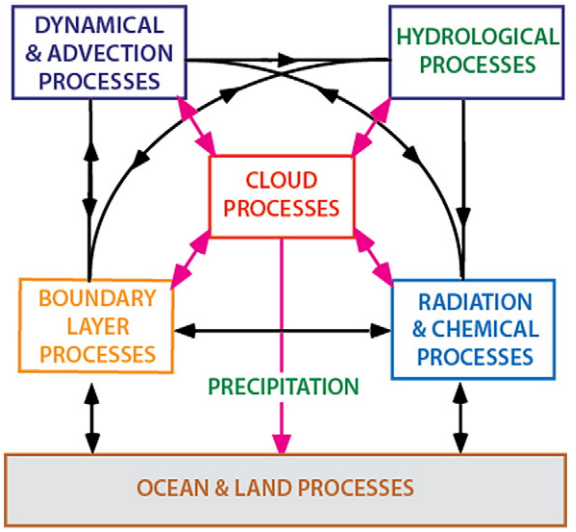

Fig. 1. Interactions between various processes in the climate system. Taken from Arakawa (2004), his Fig. 1.

Convectively active clouds play the central roles in these interactions and the problem of cumulus parameterization has always been at the core of our effort to improve numerical modeling of the atmosphere. In spite of the accumulated experience over the past decades, however, our progress in this aspect of atmospheric modeling has been especially slow (Randall et al., 2003). Besides the basic question of how to pose the problem, there are a number of uncertainties in modeling moist-convective processes as reviewed by Arakawa (2004). Even more seriously, we have not established a sufficiently general framework for representing the multiscale effects of moist-convective processes. Before the satellite age, we used to see the atmosphere through weather charts. Now we can also see the atmosphere via satellites as in the example shown in Fig. 2. Here we see lots of details as well as large-scale features. This by itself gives us the feeling that atmospheric modeling must inevitably be multiscale modeling.

In numerical modeling, we have to truncate the continuous system somewhere in the spectrum. This artificially separates the spectrum into the resolved scales, for which the local and instantaneous effects are simulated, and the unresolved scales, for which only the statistical effects can be considered through parameterization. Numerical models typically treat these two scales as separate modules as shown in Fig. 3. For the two-way interactions to take place between these modules, the loop in the figure must be closed requiring closure assumptions.

Fig. 2. An example of satellite cloud images showing clusters of clouds. Taken from http://goes.gsfc.nasa.gov/pub/goes/color_goes11d1.jpg.

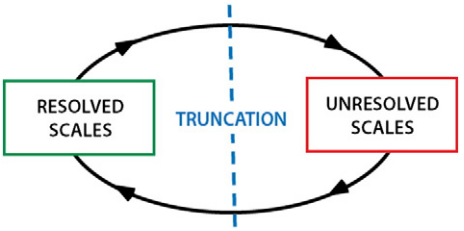

Fig. 3. A schematic diagram showing interactions between the resolved and unresolved scales separated by truncation.

Closure assumptions in the cumulus parameterization problem are reviewed by Arakawa and Chen (1987) and Arakawa (1993) in detail. The choice of a closure assumption closely reflects one's view of the parameterizability of cumulus convection, which is by no means an obvious question. One of the complexities is that cumulus parameterization in numerical modeling is more than a physical/statistical problem because it is required as a consequence of mathematical truncation. Even when the statistical effects of cumulus convection is in fact parameterizable for large grid sizes, it is highly questionable that it is also true for small grid sizes because grid-size averages themselves tend to lose their statistical significance.

Strictly speaking, truncation of a continuous system can be justified only when the resulting error can be made arbitrarily small by using a higher resolution. This requires that the dynamics and physics of the low-resolution models such as conventional general circulation models (GCMs) converge to those of the high-resolution models such as cloud-resolving models (CRMs) with an increase of the horizontal resolution. If the GCM and CRM share the same dynamics core, which must necessarily be nonhydrostatic, we expect that the convergence does take place as far as the model dynamics is concerned. Unfortunately, the same is not true for the conventional formulations of model physics especially when moist-convective processes are involved. If the model physics of GCMs is reformulated in such a way that it converges to that of CRMs, those two kinds of model physics are unified as far as the representation of deep moist convection is concerned. Then, we can freely choose intermediate resolutions or highly heterogeneous resolutions such as in local or adaptive mesh refinement, while staying with the same formulation of model physics.

The purpose of this paper is to review multiscale modeling of the moist-convective atmosphere with an emphasis of our own recent work on the subject. Section 2 presents a historical review of cumulus parameterizations with an emphasis on their physical basis. Section 3 discusses a problem in existing representations of moist-convective processes and gives a rationale for unification of model physics. Sections 4 and 5 review ROUTE I and ROUTE II for the unification, which follow the approaches of generalizing conventional cumulus parameterization and using a coupled GCM/CRM system, respectively. Finally, a summary and conclusions are presented in Section 6.

2. A historical review of cumulus parameterizations

The importance of parameterizing the large-scale effects of moist convection was recognized in the early 1960's in tropical cyclone modeling. At the first international symposium on numerical weather prediction (NWP) in Tokyo, November 1960, Akira Kasahara presented a paper on a numerical experiment to simulate the development of a tropical cyclone (Kasahara, 1962). Ironically, the experiment showed that grid-scale cumulus cells were developed instead of a cyclone-scale vortex. This result is consistent with what we know from the theories by Bjerknes (1938) and Lilly (1960), who showed that conditional instability with saturated updraft and unsaturated downdraft favors the smallest possible scale for the updraft. According to Kasahara (2000), Jule Charney gave the following comment at the end of Kasahara's presentation:

> *"…Why does a large-scale convective system form (in nature) when the motion is more unstable for cumulus-cloud scale? … We take an attitude that a hurricane or a typhoon and the cumulus clouds do not compete, but they cooperate … How do you handle that in the numerical prediction scheme and isn't it very difficult to deal with both small and large scales?"*

The idea of cooperation led Charney to propose "Conditional Instability of the Second Kind (CISK)" (Charney and Eliassen, 1964, hereafter CE64). In this paper, the authors envision that the cooperation of the two scales is through a supply of latent heat energy to the cyclone by the clouds and supplying the fuel in the form of moisture to the clouds by the low-level frictional inflow of the cyclone. No cloud model beyond the vertically integrated moisture budget is used in CE64. About the same time, Ooyama (1964, hereafter O64) independently proposed a CISK mechanism for tropical cyclone development. In contrast to CE64, O64 uses an entraining cloud model instead of requiring the moisture balance a priori. In spite of this difference, CE64 and O64 are conceptually similar in the sense that tropical cyclone development is due to the cooperation between cumulus- and cyclone-scale motions through frictionally induced cyclone-scale convergence on one hand and energy supply by cumulus heating on the other hand.

The idea of CISK as multiscale modeling of the moist-convective atmosphere subsequently became popular among the tropical meteorology community. It has been, however, subject to criticisms also. Perhaps one of the most severe criticisms is that of Emanuel et al. (1994), who pointed out that the release of latent heat does not necessarily generate kinetic energy. Arakawa (2004) also criticized the idea of the low-level convergence as a cause for cyclone development. The low-level convergence brings drier and colder air of the outer region into the central region, decreasing the low-level equivalent potential temperature θ_e of the latter region. From the point of view of conditional instability, this is a negative feedback. More fundamentally, cooperation of cyclone- and cumulus-scale motions without external sources can never explain the intensification of the central warm core during the cyclone development. This is because motion under moist-adiabatic processes simply redistributes θ_e without creating a new value.

Ooyama's subsequent work (Ooyama, 1969), however, can be considered as the first successful numerical simulation of tropical cyclone development. The model used is basically a nonlinear version of that used in O64, but very importantly, the low-level θ_e is now predicted with the effect of the surface

heat fluxes. Then, as in the Wind-Induced Surface Heat Exchange (WISHE) theory later proposed by Emanuel (1986), the surface heat flux can be enhanced as the cyclone develops due to stronger surface wind. If a quasi-neutral vertical profile is assumed, this means that θ_e is increased at all levels, which is a positive feedback on the cyclone development. For more details of the early history of cumulus parameterization in tropical cyclone modeling, see Section 3 of Arakawa (2004).

Cumulus parameterization in GCMs has a quite different history, beginning with the introduction of moist-convective adjustment into a GCM by Manabe et al. (1965) (hereafter M65). Although the concept of moist-convective adjustment was not necessarily new (e.g., Smagorinsky, 1956; Mintz, 1958), M65 represents the first application of this concept to a numerical model of the moist atmosphere. Fig. 4(a) schematically illustrates the adjustment process using an idealized model that consists of only the planetary boundary layer and a tropospheric layer. The abscissa is the mean temperature lapse rate Γ between the two layers, Γ_m and Γ_d are the moist-adiabatic and dry-adiabatic lapse rates, respectively, and the ordinate is the relative humidity RH of the layers. The horizontal solid line at $RH=1$ with $\Gamma<\Gamma_m$ represents the critical relative humidity for non-convective condensation. If the air tends to be in the yellow quadrant, this type of condensation takes place and RH is adjusted to 1. The solid dot represents the saturated neutral state, which is the equilibrium point used in M65. If the air tends to be in the pink quadrant due to the forcing by other processes, both Γ and RH are instantaneously adjusted to the dot point as shown by the red and green arrows. Conservation of the moist static energy defined by $h \equiv cpT + Lq + gz$, where c_pT, Lq and gz are the sensible heat, latent heat and geopotential energy, respectively, uniquely determines the mean temperature of the layers after the adjustment.

The moist-convective adjustment of M65 can easily be criticized because the adjustment takes place only when the air tends to be super-saturated. Using a three-level model, Arakawa (1969, hereafter A69) introduced a more general definition of neutral states characterized by $A=0$, where A is a measure of moist-convective instability that depends on the low-level relative humidity as well as the temperature lapse rate. For these neutral states, generally $RH<1$ and $\Gamma>\Gamma_m$ as schematically shown by the dashed line in Fig. 4(b). Whenever the air tends to enter the pink area with $A>0$ due to the forcing by other processes, adjustment to the $A=0$ line takes place. In general, the destination point of adjustment is not the same as the departure point of forcing as shown by the red and green arrows. Thus the adjusted state can move along the dashed line with time and thus the line should be interpreted as a quasi-equilibrium line rather than an ensemble of equilibrium points. This is a prototype of the quasi-equilibrium hypothesis postulated by Arakawa and Schubert (1974).

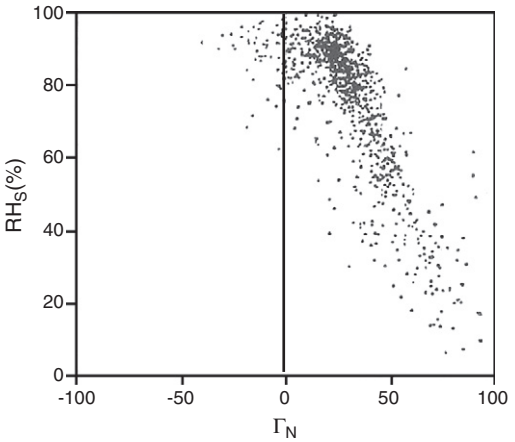

Fig. 5. Plots of the normalized lapse rate defined by $\Gamma_N \equiv (\Gamma-\Gamma_m)/(\Gamma-\Gamma_d)$ vs. the surface relative humidity RH_s.
Taken from Arakawa and Chen (1987), their Fig. 11.

There is observational evidence for the existence of quasi-equilibrium states similar to the dashed line shown in Fig. 4(b). Fig. 5 shows such an example given by Arakawa and Chen (1987). Here the abscissa is a normalized lapse rate defined by $\Gamma_N \equiv (\Gamma-\Gamma_m)/(\Gamma-\Gamma_d)$, Γ is now the mean lapse rate between the surface and 500 hPa, and the ordinate is the surface relative humidity RH_s. The data used for these plots is obtained from a gridded dataset over Southeast Asia. For more details of the dataset, see Arakawa and Chen (1987). Although the scatter is large, the figure clearly shows clustering of the plots around a quasi-equilibrium line similar to the dashed line in Fig. 4(b). [The quasi-equilibrium line may be closer to the $\Gamma_N=0$ line for the cloud regimes with dominant shallow clouds].

Betts and Miller (Betts and Miller, 1986; see also Betts, 1986; Betts and Miller, 1993) later proposed an adjustment

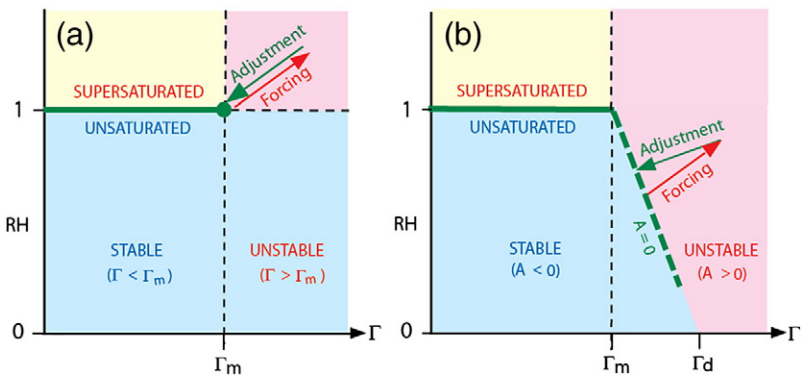

Fig. 4. A schematic illustration of the equilibrium states, forcing and adjustment for (a) M65 and (b) A69, where Γ is the mean temperature lapse rate between the boundary layer and a tropospheric layer, Γ_m and Γ_d are the moist-adiabatic and dry-adiabatic lapse rates, respectively, and RH is the relative humidity of the layers.

scheme for cumulus parameterization. In contrast to A69, the Betts–Miller scheme specifies equilibrium profiles for temperature and humidity semi-empirically. The scheme is popular perhaps because it is simple and flexible while maintaining the essence of the cumulus effects that need to be parameterized.

Many GCMs and NWP models, however, have used various versions of the parameterization proposed by Kuo (1974, hereafter K74). In this scheme, as in CE64, the moisture convergence by resolved motion controls the heating due to unresolved cumulus convection through the moisture budget. It should be noted, however, that the use of the moisture budget equation for parameterization means that the equation cannot be used again for prediction. Thus the predictability of the moisture field is lost. This is why Kuo's parameterization has to introduce a disposal parameter for the participation of the converged water vapor between the moistening and precipitating parts. Partly due to this, K74 was severely criticized by Emanuel and Raymond (1992), Raymond and Emanuel (1993), Emanuel (1994) and Emanuel et al. (1994). In spite of these criticisms, however, we should not ignore the fact that the K74 scheme can produce acceptable results in many practical applications. The key to understand this paradox is that the scheme can also be viewed as an adjustment scheme, as Arakawa (2004) pointed out, though the choice of the adjustment time scale can hardly be justified. In any case, this is an example showing that the performance of a parameterization scheme may be better understood by deviating from its author's own rationale for the scheme.

The quasi-equilibrium hypothesis is further elaborated by Arakawa and Schubert (1974, hereafter AS; see Arakawa and Cheng, 1993 and Randall et al., 1997a for reviews). AS considers a cloud ensemble that consists of a spectrum of cloud types as shown in Fig. 6 for a portion of the horizontal domain. The hypothesis follows two logical steps below:

STEP I. As in Lord and Arakawa (1980), the following kinetic energy equation is considered for each cloud type:

$$dK/dt = M(A-\delta), \tag{2.1}$$

where K is the kinetic energy of the motion associated with the clouds, M is the total vertical mass flux by the clouds, A is the cloud work function defined as the rate of kinetic energy generation by the buoyancy force per unit M, and δ is the rate of kinetic energy dissipation per unit M. The cloud work function is an integral measure of moist-convective instability that depends on the vertical distributions of temperature and humidity. It is similar to the convective available potential energy CAPE but depends on the cloud type classified in terms of the fractional rate of entrainment. The neutral states can then be defined as the vertical structures that satisfy the kinetic energy equilibrium given by

$$A = \delta. \tag{2.2}$$

These neutral states should look similar to the dashed line in Fig. 4(b) except that δ is not neglected now. STEP I assumes that the cloud ensemble tends to adjust the environment to establish a neutral state whenever the situation $A>\delta$ occurs.

STEP II. AS then considers the time derivative of A in the form of

$$dA/dt = (dA/dt)_{LS} + (dA/dt)_{CU}, \tag{2.3}$$

where the first and second terms on the right hand side represent dA/dt due to the large-scale and cumulus processes, respectively. The situation $(dA/dt)_{LS}>0$ acting on the state $A=\delta$ means destabilization or forcing due to the large-scale processes. In such a situation, $(dA/dt)_{CU}<0$ is assumed from STEP I, which is self-stabilization or adjustment to the state $A=\delta$ due to cumulus processes. STEP II then assumes the cloud work function equilibrium given by

$$(dA/dt)_{CU} = -(dA/dt)_{LS}. \tag{2.4}$$

The assumption in Eq. (2.4) can be justified when the adjustment takes place sufficiently fast compared to the evolution of $(dA/dt)_{LS}$. Since $(dA/dt)_{CU}$ depends on

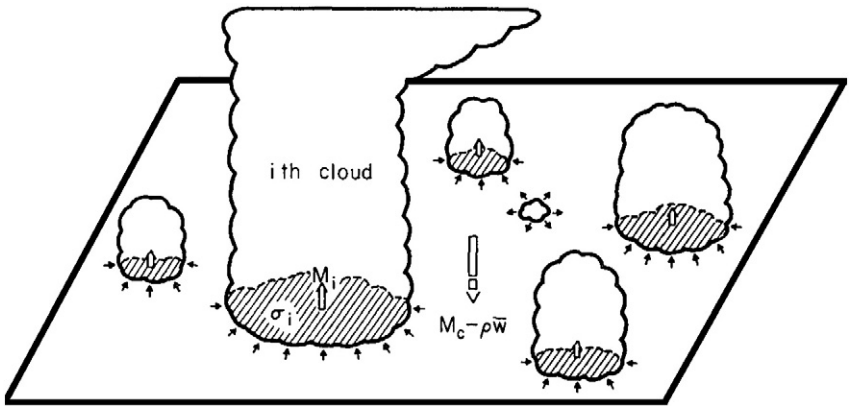

Fig. 6. A horizontal area at a tropospheric level showing different types of penetrating clouds with entrainment, detrainment and subsidence in the environment. Taken from AS, their Fig. 1.

the cumulus mass flux M, Eq. (2.4) determines M necessary to maintain the cloud work function equilibrium. For observational evidence of the quasi-equilibrium, see AS and Randall et al. (1997b).

The quasi-equilibrium hypothesis discussed here is used by AS as the principal closure. It seems that the majority of GCMs now use this type of principal closure, often considering a single cloud type and/or CAPE instead of the cloud work function. Also, many parameterizations use relaxed adjustment, in which the adjustment given by the left hand side of Eq. (2.4) is relaxed to a fraction of the forcing given by the right hand side. Examples include the widely used parameterizations by Kain and Fritsch for mesoscales (Kain and Fritsch, 1990, 1993, 1998) and the relaxed Arakawa–Schubert (RAS) proposed by Moorthi and Suarez (1992).

To a large extent, the history of cumulus parameterization has been designing, revising, evaluating and tuning of closure assumptions, cloud models, and formulations of convective triggering. Practically all of these efforts are, however, based on the modular structure illustrated in Fig. 3. In our opinion, the history has reached the stage at which we should seriously question the impact of this artificial separation of the spectrum as we discuss in the next section.

3. Rationale for unification of model physics

This and next two sections discuss the rationale and two possible approaches for unifying multiscale representations of moist convection in numerical models of the atmosphere. The rationale for the unification comes from the following assessment of the current status of atmospheric modeling by Arakawa et al. (2011): As far as representation of deep moist convection is concerned, only two kinds of model physics are used at present: *highly parameterized* and *explicitly simulated*. Correspondingly, besides those models that explicitly simulate turbulence such as Direct Numerical Simulation and Large Eddy Simulation models, we have two discrete families of atmospheric models as shown in Fig. 7, one represented by GCMs and the other by CRMs. In this figure, the abscissa is the horizontal resolution and the ordinate is a measure for the degree of parameterization, such as the reduction in the degrees of freedom, increasing downwards.

Naturally, there have been many studies to examine the applicability of GCMs to higher resolutions as shown by the horizontal arrow in Fig. 7. Among those studies, the work of Williamson (1999) is particularly intriguing. The paper shows that, when the horizontal resolution of the NCAR CCM2 is increased for both the dynamics and physical parameterizations, the upward branch of the Hadley circulations increases in strength and there is no sign of convergence. When the horizontal resolution is increased for the dynamics but not for the parameterizations, the solution converges. But the converged state is similar to that obtained with the coarse resolution for both so that the increased resolution for the dynamics is wasted. Together with other evidence, he concludes,

> "*the results raise a serious question — are the parameterizations correctly formulated in the model ? … The parameterizations should explicitly take into account the scale of the grid on which it is based.*"

Fig. 8 schematically illustrates the difference of model physics between the two families of models. For a given observed large-scale condition, we can identify the *apparent heat source*, Q_1, and the *apparent moisture sink*, Q_2, from the residuals in the large-scale heat and moisture budgets as in the analysis presented by Yanai et al. (1973). Here the heat source and moisture sink refer to the source of the sensible heat c_pT and the sink of the latent heat Lq, respectively. In such an analysis, the direction of the lower half of the loop shown in Fig. 3 is reversed. In spite of this, or rather because of this, the results are useful to infer what the effects of unresolved moist convection are in the real atmosphere. The left panel of Fig. 8 schematically shows typical profiles of Q_1, Q_2 and $Q_1 - Q_2$ for disturbed tropical conditions. The difference $Q_1 - Q_2$ gives the *apparent moist static energy source*. As shown in the figure, the profile of $Q_1 - Q_2$ typically has negative values in the lower troposphere and positive values in the middle to upper

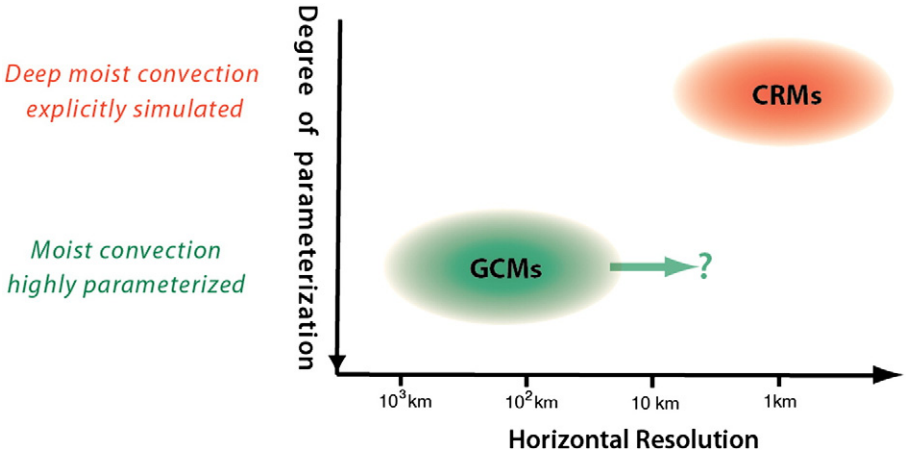

Fig. 7. Two families of atmospheric models currently being used. The horizontal arrow represents attempts to broaden the applicability of GCMs to higher resolutions.

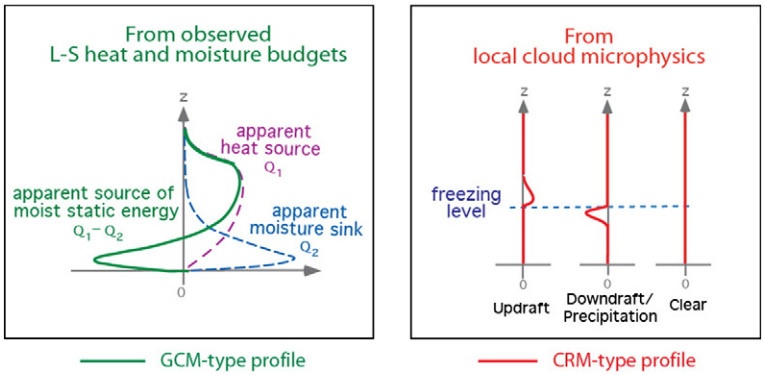

Fig. 8. Schematic illustration of typical profiles of moist static energy source. The heavy line in left panel: source required for low-resolution models such as GCMs as suggested by observed large-scale budgets. Right panel: source required for high-resolution models such as CRMs as expected from local cloud microphysics. Redrawn from Arakawa (2004), his Fig. 9.

troposphere, indicating the dominant role of vertical eddy transport of moist static energy. When deep moist convection is dominant, cumulus parameterization in GCMs is expected to produce this type of profiles, which we call the "GCM-type". The existing cumulus parameterizations are generally capable of producing this type of profiles.

In contrast, the local cloud microphysical processes produce practically no moist static energy source/sink except near the freezing level. This is because moist static energy is conserved under moist-adiabatic processes and thus it has no significant source/sink except where the ice phase is involved. Within updrafts and downdrafts/precipitation, there are sources immediately above the freezing level due to freezing and sinks immediately below that level due to melting, respectively. This is illustrated in the right panel of Fig. 8. Cloud microphysics in CRMs is expected to produce this type of profiles, which we call the "CRM-type". Here it is important to recognize that any space/time/ensemble average of the CRM-type profiles does not give a GCM-type profile, suggesting that the cumulus parameterization problem is more than a statistical theory of cloud microphysics.

Due to the advance of computer technology, we can afford increasingly higher horizontal resolutions for numerical models of the atmosphere. Even a global cloud-resolving model (GCRM, e.g., Sato et al., 2009), which explicitly simulates the "true" heat source and moisture sink, can now be used for climate simulations. This means that there is a tendency toward bipolarization of global models since conventional GCMs and GCRMs have qualitatively different model physics as we have seen in Fig. 8. Ideally, GCMs should converge to GCRMs as the resolution is refined so that intermediate resolutions can be freely chosen without changing the formulation of model physics.

Jung and Arakawa (2004) performed budget analyses of data simulated by a CRM with different space/time resolutions and with and without the cloud-microphysics component of the CRM. By comparing the results of the low-resolution runs without cloud microphysics with that of the high-resolution run with cloud microphysics (CONTROL), the apparent source required for the low-resolution models is identified. This procedure is repeated over many realizations selected from CONTROL and then the ensemble average is taken. For illustration, the results are further space averaged over the entire model domain.

Fig. 9 shows examples of the domain- and ensemble-averaged profiles of "required" cloud-microphysical source

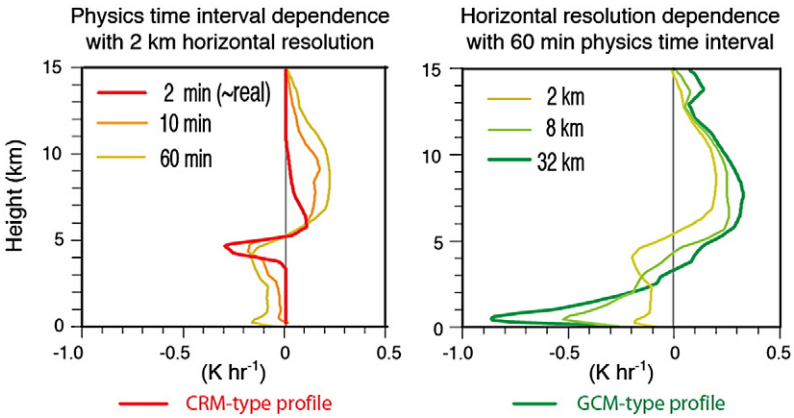

Fig. 9. Domain- and ensemble-averaged profiles of the "required source" for moist static energy due to cloud microphysics under strong large-scale forcing over land. Left panel: dependency on physics time interval with a fixed horizontal grid size (2 km). Right panel: dependency on horizontal grid size with a fixed physics time interval (60 min).
From Jung and Arakawa (2004).

of moist static energy. The left panel shows those with the same horizontal grid size as that used for CONTROL (2 km) but with different time intervals of implementing cloud microphysics. The heavy red line is for the case with a small time interval (2 min), approximately representing the "real" source. Note that, as expected, this line resembles a mixture of the CRM-type profiles shown in the right panel of Fig. 8. We see that, as the time interval becomes longer, the peaks localized in the real source are dispersed in the required source both upward and downward. This dependence of the required source on the physics time interval must be due to the upward transports of air with high moist static energy produced by freezing in updrafts and downward transports of air with low moist static energy produced by melting in precipitating downdrafts. The right panel, on the other hand, shows the horizontal-resolution dependence of domain- and ensemble-averaged profiles of the required source of moist static energy for a fixed physics time interval (60 min) but for different horizontal grid sizes. We see that the peaks of the required source for larger grid sizes considerably deviate from those for the 2 km grid size. With the 32 km grid size shown by the heavy green line, for example, we see a pronounced sink in the lower troposphere and a pronounced source spread throughout the middle and upper troposphere, resembling the GCM-type profile shown in the left panel of Fig. 8.

Fig. 10 is the same as Fig. 9 but for the required cloud-microphysical source of total (airborne) water mixing ratio. The left panel shows dominant sinks in the middle troposphere due to the generation of precipitating particles and small peaks of source near the surface due to the evaporation from precipitation. These features do not significantly depend on the physics time interval. The right panel, however, shows a strong dependency of the (negative) source on the horizontal grid size, again due to the existence of vertical transports by deep convective systems.

The existence of the in-between profiles shown in these figures by the thin lines strongly suggests that the required model physics smoothly transitions from one type to the other as the resolution changes. As we have seen in these figures, the required sources highly depend on the horizontal resolution of the model, as well as on the time interval for implementing physics in the case of moist static energy. The formulation of model physics should automatically reproduce these dependences as it is applied to different resolutions. Conventional cloud parameterization schemes, however, cannot do this because they assume either explicitly or implicitly that the horizontal grid size and the time interval for implementing physics are sufficiently larger and longer than the size and lifetime of individual moist-convective elements. This generates difficulties in high-resolution models, in which grid-scale and subgrid-scale moist processes are not well separable, as is typical in mesoscale models (Molinari and Dudek, 1992; see also Molinari, 1993 and Frank, 1993). If the model physics of GCMs is reformulated to produce such transitions, GCMs and CRMs including mesoscale models are unified to a single family of models that can cover a wide range of horizontal resolutions with the same formulation of model physics.

We can think of two routes to achieve the unification of the two families of models. ROUTE I continues to follow the parameterization approach, but uses a unified parameterization with which the GCM converges to a global CRM (GCRM) as the grid size is refined. On the other hand, ROUTE II replaces the parameterization of deep moist convection with a partial simulation of cloud-scale processes by CRMs and formulates the coupling of GCM and CRMs in such a way that the coupled system formally converges to a GCRM as the GCM grid size is refined. These two routes are reviewed in the next two sections.

4. ROUTE I for the unification — the unified parameterization

This section reviews ROUTE I for the unification mainly following Arakawa et al. (2011, hereafter AJW11) with some updates.

4.1. Identification of the problem

To identify the problem to be addressed in ROUTE I, we use the AS parameterization as an example of the starting point. AS says,

> "*Consider a horizontal area — large enough to contain an ensemble of cumulus clouds but small enough to cover a fraction of a large-scale disturbance. The existence of such an area is one of the basic assumptions of this paper.*"

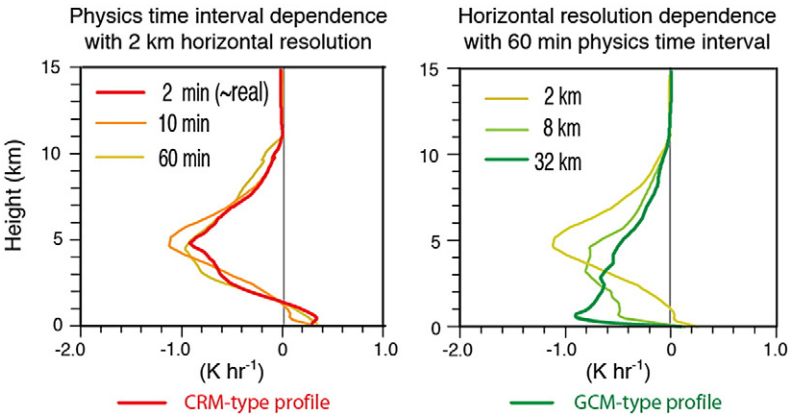

Fig. 10. Same as Fig. 9 but for total (airborne) water.

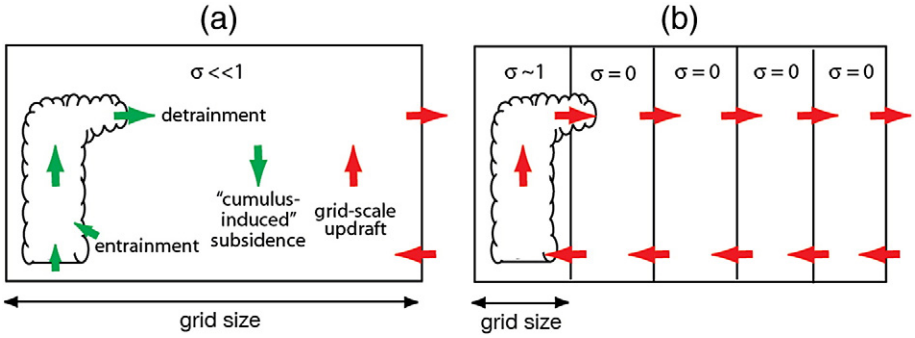

Fig. 11. Schematic illustration of circulations associated with clouds for (a) coarse and (b) fine resolutions. Taken from AJW11, their Fig. 5.

This assumption is commonly used in most conventional cumulus parameterizations either explicitly or implicitly. In reality, however, the GCM grid cells are not large enough and, at the same time, not small enough.

Many mass-flux based parameterizations (e.g., AS, Tiedtke, 1989; Kain and Fritsch, 1990; Gregory and Rowntree, 1990; Emanuel, 1991; Zhang and McFarlane, 1995) assume, at least implicitly, that convective clouds cover only a small portion of the GCM grid cell. With this assumption, the temperature and water vapor to be predicted are essentially those for the cloud environment. Then, as illustrated by the green arrows in Fig. 11(a), relevant physical processes are the "cumulus-induced" subsidence in the environment and the detrainment of cloud air into the environment.

Here it is important to note that the "cumulus-induced subsidence" is only a hypothetical subsidence. It is a component of the *subgrid-scale eddy*, which has its own mass budget closed within the same grid cell by definition. This does not mean that the true subsidence is confined within that cell. The true subsidence is the sum of the green and red vertical arrows in Fig. 11(a), which normally tend to compensate each other. In such a case, the true subsidence occurs in another grid cell, which may well be far away, whose position is determined by the grid-scale dynamics, not by the parameterization. This point is often misunderstood in the literature.

As the grid size becomes smaller, the cloud may eventually occupy the entire grid cell so that there is no "environment" within the same cell. The updraft through the cloud then becomes a part of gird-scale circulation as shown in Fig. 11(b). In this situation, cumulus parameterization should not play any role because it is supposed to be a formulation of the *subgrid-scale eddy* effects. The probability density distribution of the fractional convective cloudiness σ becomes bimodal in this limit, consisting of $\sigma=1$ and $\sigma=0$ (Krueger, 2002; Krueger and Luo, 2004). It is then clear that a key to unify the parameterizations in GCMs and CRMs is to include a transition to this limit by eliminating the assumption of $\sigma<<1$.

For visualization of the problem raised above, we have analyzed datasets simulated by a 3D CRM applied to a horizontal domain of 512 km × 512 km with a 2 km grid size. Other experimental settings are similar to the benchmark simulations performed by Jung and Arakawa (2010). Two 24-hour simulations are made, one with and the other without background shear. Fig. 12 shows snapshots of vertical velocity w at 3 km height at the end of these simulations. As is clear from the figure, the two simulations represent quite different cloud regimes. For the analysis presented in the rest of this section, datasets are taken from the last 2-hour period of each simulation with 20-min intervals. To represent the grid cells of GCMs, the domain is divided into sub-domains

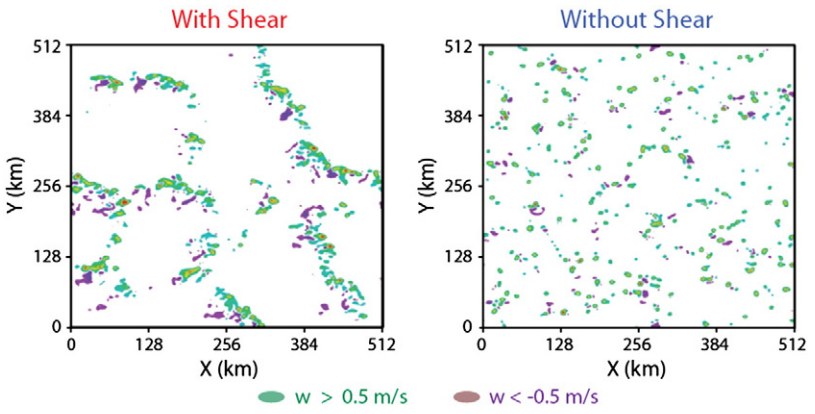

Fig. 12. Snapshots of vertical velocity w at 3 km height at the end of two simulations with and without background shear. Taken from AJW11, their Fig. 6.

of equal size. These sub-domains are then used to analyze the resolution dependency of the statistics of data. The selected side lengths of the sub-domains are $d_n = 512\ km/2^{n-1}$, $n = 2, 3, 4, .., 9$. Fig. 13 shows the original ($n = 1$) and examples of the sub-domains.

In the analysis, grid points that satisfy $w > 0.5$ m/s are considered as "cloud points". The fractional convective cloudiness σ can then be diagnosed from the fractional number of cloud points in the sub-domain. Let $\langle X \rangle$ be the average of X over all cloud-containing (i.e., $\sigma \neq 0$) sub-domains of the same size, where X is a variable defined for each sub-domain. Fig. 14 shows $\langle \sigma \rangle$ and its standard deviation at 3 km height against d_n for the shear case (a) and non-shear case (b). It is clear that $\sigma << 1$ can be a good approximation only when coarse resolutions are used. The value of $\langle \sigma \rangle$ tends to increase as d_n decreases and becomes 1 for $d_n = 2$ km, which is the grid size of the CRM used. The standard deviation is large for high resolutions, but it is expected since there is no reason to believe that σ is a unique function of d_n. In spite of the large standard deviation, the tendency toward a bimodal distribution of $\sigma = 1$ and $\sigma = 0$ can be seen for high resolutions.

Recall that the vertical eddy transport of moist static energy is responsible for the difference between the GCM-type and CRM-type profiles illustrated in Fig. 8. Let an overbar denote the mean over the entire area of a sub-domain. Then the vertical eddy transport of a thermodynamic variable ψ per unit horizontal area and density (hereafter eddy transport) for the sub-domain is given by $\overline{w\psi} - \overline{w}\,\overline{\psi}$. This quantity is zero if there are no clouds and the cloud environment is horizontally uniform. Even if the sub-domain contains a cloud, it should be zero for $d_n = 2$ km because there is no room for eddies. Fig. 15 shows vertical profiles of the eddy transport of moist static energy $\overline{wh} - \overline{w}\,\overline{h}$ diagnosed for each sub-domain and then averaged over all sub-domains of the same size. The figure shows that, for both the shear and non-shear cases, the averaged eddy transport monotonically decreases as the sub-domain size d_n decreases, ending up to zero for $d_n = 2$ km. It should be remembered that Fig. 15 shows the eddy transport averaged over *all* sub-domains of the same size. This average is what matters for the budget of the entire domain. As it can be seen later, the dependence on d_n is quite different from that shown in Fig. 15 if the average is taken only over the cloud-containing sub-domains.

4.2. Expressions for the eddy transport

As is commonly done in the conventional cumulus parameterizations, we assume that the cloud and environment values of ψ denoted by ψ_c and $\tilde{\psi}$, respectively, are horizontally uniform individually. Further, let w_c and $\tilde{w}$ be the averages of w over the clouds and the environment, respectively. The effect of convective-scale downdrafts is ignored at this stage of development. Denoting the mean over the entire area of a grid cell by an overbar, AJW11 derived the following expression for the eddy transport of ψ:

$$\overline{w\psi} - \overline{w}\,\overline{\psi} = \frac{\sigma}{1-\sigma}(w_c - \overline{w})(\psi_c - \overline{\psi}). \tag{4.1}$$

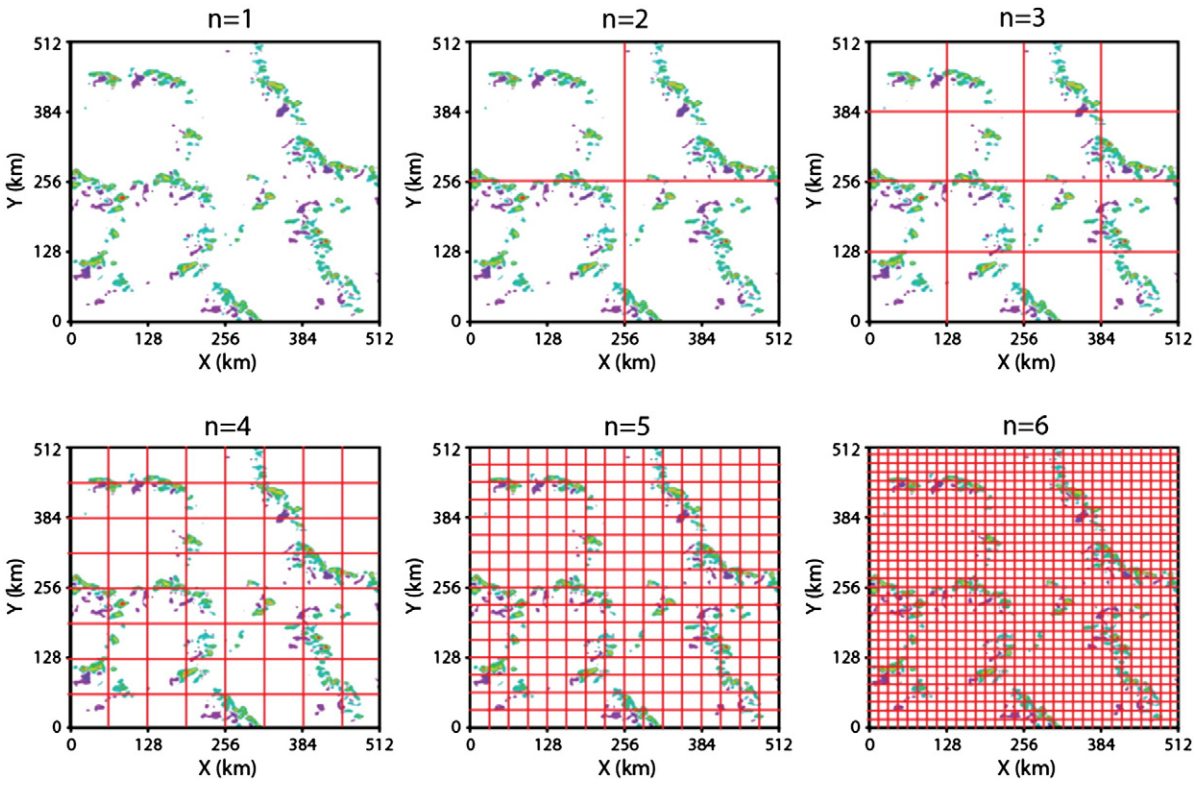

Fig. 13. The original domain and examples of the sub-domains used for analysis. The background field is same as the left panel of Fig. 12. Taken from AJW11, their Fig. 7.

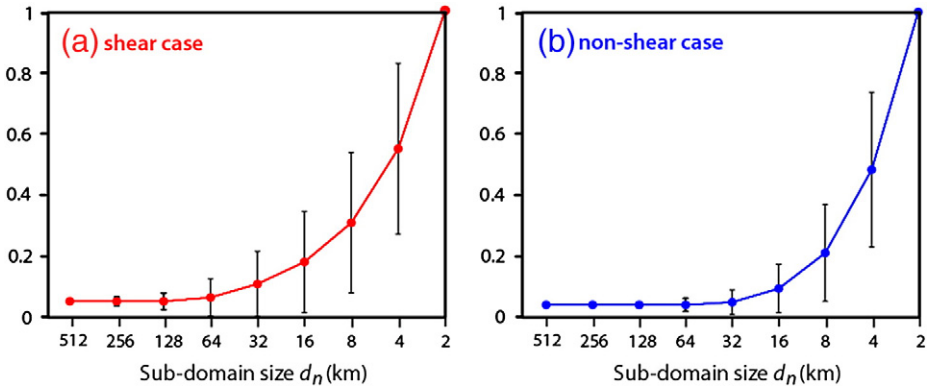

Fig. 14. The sub-domain size dependence of σ averaged over cloud-containing sub-domains and its standard deviation at 3 km height. Taken from AJW11, their Fig. 8.

If $\sigma<<1$ and $|\overline{w}|<<w_c$ are assumed, Eq. (4.1) can be approximated as

$$\rho(\overline{w\psi}-\overline{w}\,\overline{\psi})\approx M_c(\psi_c-\overline{\psi}), \tag{4.2}$$

where $M_c\equiv\rho\sigma w_c$ is the cloud mass flux. Most conventional parameterizations based on mass-flux effectively use this expression [see, for example, (35) and (36) of AS], which indicates that the cloud vertical velocity w_c matters only through the product σw_c in M_c as far as the eddy transport is concerned. This is not the case if the assumption $\sigma<<1$ is eliminated. Thus the unified parameterization must determine both σ and w_c.

The requirement that the parameterization converge to an explicit simulation of cloud processes as $\sigma\to 1$ is

$$\lim_{\sigma\to 1} w_c=\overline{w} \text{ and } \lim_{\sigma\to 1}\psi_c=\overline{\psi}. \tag{4.3}$$

Thus, $w_c-\overline{w}$ and $\psi_c-\overline{\psi}$ are of the order of $1-\sigma$ (or higher) so that $(w_c-\overline{w})(\psi_c-\overline{\psi})$ is of the order of $(1-\sigma)^2$ (or higher) near this limit. The simplest choice to satisfy this requirement is

$$(w_c-\overline{w})\left(\psi_c-\overline{\psi}\right)=(1-\sigma)^2\left[(w_c-\overline{w})(\psi_c-\overline{\psi})\right]^*, \tag{4.4}$$

where an asterisk denotes the value expected when $\sigma<<1$, which can be estimated with a one-dimensional model for a single cloud. We can show that this choice is equivalent to the assumption that $(w_c-\tilde{w})\left(\psi_c-\tilde{\psi}\right)$ is independent of σ, where a tilde denotes the value of the cloud environment. Substituting Eq. (4.4) into Eq. (4.1), we obtain

$$\overline{w\psi}-\overline{w}\,\overline{\psi}=\sigma(1-\sigma)\left[(w_c-\overline{w})(\psi_c-\overline{\psi})\right]^*. \tag{4.5}$$

Since $\left[(w_c-\overline{w})(\psi_c-\overline{\psi})\right]^*$ does not depend on σ by definition, Eq. (4.5) shows that the dependence of $\overline{w\psi}-\overline{w}\,\overline{\psi}$ on σ is only through the factor $\sigma(1-\sigma)$. This equation represents the basic structure of the unified parameterization.

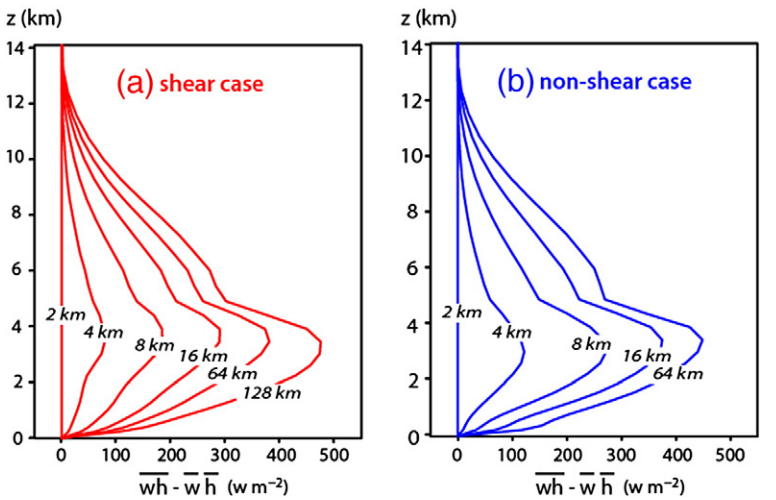

Fig. 15. Vertical profiles of the vertical eddy transport of moist static energy averaged over all sub-domains for each value of the sub-domain size d_n.

4.3. Partial evaluation of the unified parameterization

At this stage, we present a partial evaluation of the unified parameterization using the dataset mentioned in Subsection 4.1. It is designed to evaluate the formal structures of Eqs. (4.4) and (4.5) with the moist static energy h as an example of ψ. With $\psi = h$, the averages of Eqs. (4.4) and (4.5) over all *cloud-containing* sub-domains of the same size are given by

$$\langle (w_c-\overline{w})\left(h_c-\overline{h}\right)\rangle = \langle (1-\sigma)^2\rangle \left[(w_c-\overline{w})\left(h_c-\overline{h}\right)\right]^* \tag{4.6}$$

and

$$\langle \overline{wh}-\overline{w}\,\overline{h}\rangle = \langle \sigma(1-\sigma)\rangle \left[(w_c-\overline{w})\left(h_c-\overline{h}\right)\right]^*, \tag{4.7}$$

respectively. Here the difference of $\left[(w_c-\overline{w})\left(h_c-\overline{h}\right)\right]^*$ between the sub-domains is ignored. Since this quantity cannot be directly diagnosed from the dataset, it is eliminated between Eqs. (4.6) and (4.7) to obtain

$$\langle \overline{wh}-\overline{w}\overline{h}\rangle = \frac{\langle \sigma(1-\sigma)\rangle}{\langle (1-\sigma)^2\rangle}\ \langle (w_c-\overline{w})\left(h_c-\overline{h}\right)\rangle. \tag{4.8}$$

The solid and open circles in Fig. 16 show the diagnosed values of the left and right hand sides of Eq. (4.8) at 3 km height for each sub-domain size d_n. These values have peaks in the mesoscale range because they are small for low resolutions with $\sigma \ll 1$ and for high resolutions with $\sigma \sim 1$. Amazingly, the resolution dependence of the values estimated using the right hand side is very similar to that directly diagnosed using the left hand side. The magnitudes of the estimated values are, however, systematically smaller than those of the directly diagnosed ones. This is not surprising in view of the various idealizations used in deriving the right hand side, such as neglecting convective downdrafts, internal structure of clouds, cloud organizations, and possible coexistence of different types of clouds and different phases of cloud development. Moreover, the somewhat arbitrarily chosen criterion $w > 0.5$ m/s for cloud points influences the estimated values but not the directly diagnosed values. In any case, these results provide evidence that the formal structure of the unified parameterization is basically valid even from the resolution-dependence point of view.

4.4. Determination of σ and additional comments

The closure of conventional cumulus parameterizations determines the apparent source of thermodynamic prognostic variables. For ψ, it is given by $S_\psi - \partial\rho(\overline{w\psi}-\overline{w}\,\overline{\psi})/\rho\partial z$, where S_ψ is the true source of ψ per unit mass due to sub-grid cloud processes and ρ is the density. From this together with S_ψ determined by the parameterization, the eddy transport $(\overline{w\psi}-\overline{w}\,\overline{\psi})$ can be calculated. Let the value of $(\overline{w\psi}-\overline{w}\,\overline{\psi})$ calculated in this way with full adjustment to a quasi-equilibrium state be $(\overline{w\psi}-\overline{w}\,\overline{\psi})_{adj}$. For this value of $(\overline{w\psi}-\overline{w}\,\overline{\psi})$ to be consistent with the value of $\left[(w_c-\overline{w})(\psi_c-\overline{\psi})\right]^*$ estimated with the cloud model, Eq. (4.1) requires

$$(\overline{w\psi}-\overline{w}\,\overline{\psi})_{adj} = \frac{\sigma}{1-\sigma}\left[(w_c-\overline{w})(\psi_c-\overline{\psi})\right]^* \tag{4.9}$$

and thus σ must be such that

$$\sigma = \frac{(\overline{w\psi}-\overline{w}\,\overline{\psi})_{adj}}{(\overline{w\psi}-\overline{w}\,\overline{\psi})_{adj} + \left[(w_c-\overline{w})(\psi_c-\overline{\psi})\right]^*}. \tag{4.10}$$

It can be seen that the condition $0 \le \sigma \le 1$ is automatically satisfied by Eq. (4.10) as long as both $(\overline{w\psi}-\overline{w}\,\overline{\psi})_{adj}$ and $\left[(w_c-\overline{w})(\psi_c-\overline{\psi})\right]^*$ have the same sign, with $\sigma \to 0$ as $(\overline{w\psi}-\overline{w}\,\overline{\psi})_{adj} \to 0$ and $\sigma \to 1$ as $(\overline{w\psi}-\overline{w}\,\overline{\psi})_{adj} \to \infty$. The unified parameterization uses σ determined in this way with a selected thermodynamic variable for ψ. Since the objective is to determine σ for use in formulating the eddy transport, it is good to select a quasi-conservative variable such as h for ψ, for which S_ψ is small. As far as the basic reasoning is concerned, this approach of determining σ is in parallel to Emanuel (1991) in the sense that the following two are combined: vertical profiles of cloud properties determined by a cloud model and the total vertical transport necessary for the adjustment to a quasi-equilibrium.

Finally, elimination of $\left[(w_c-\overline{w})(\psi_c-\overline{\psi})\right]^*$ between Eqs. (4.5) and (4.9) gives

$$\overline{w\psi}-\overline{w}\,\overline{\psi} = (1-\sigma)^2(\overline{w\psi}-\overline{w}\,\overline{\psi})_{adj}. \tag{4.11}$$

This is the equation that can be used in practical applications. As expected, the right hand side of Eq. (4.11) becomes

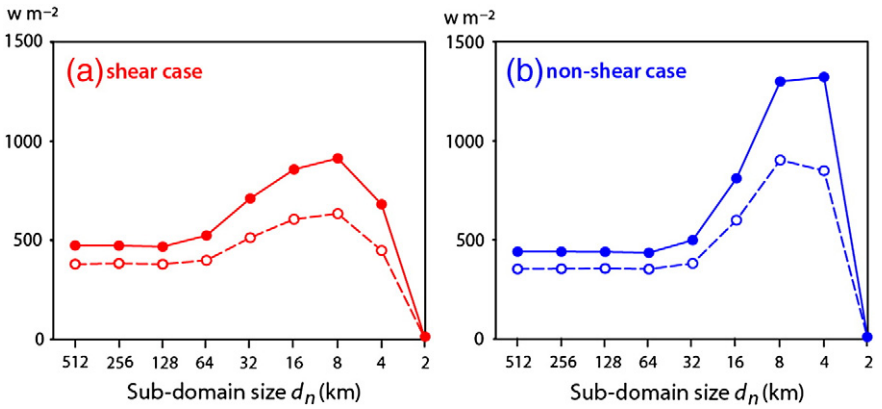

Fig. 16. The sub-domain size dependence of vertical eddy transport of moist static energy averaged over all cloud-containing sub-domains at 3 km height diagnosed with the left-hand (solid circles) and right-hand (open circles) sides of Eq. (4.8).

$\left(\overline{w\psi}-\overline{w}\,\overline{\psi}\right)_{adj}$ when $\sigma \ll 1$. When σ is finite, Eq. (4.11) shows that the actual eddy transport is less than $\left(\overline{w\psi}-\overline{w}\,\overline{\psi}\right)_{adj}$, indicating that the adjustment is relaxed as in the relaxed Arakawa–Schubert parameterization (Moorthi and Suarez, 1992). The factor $(1-\sigma)^2$ means that the amount of relaxation increases as σ increases and thus leaves a more room for explicit simulation of the transports.

A good cloud model to determine $\left[(w_c-\overline{w})(\psi_c-\overline{\psi})\right]^*$ and a reasonable closure to determine the magnitude of $\left(\overline{w\psi}-\overline{w}\,\overline{\psi}\right)_{adj}$ are prerequisites to the success of the unified parameterization. Also, dynamics and the formulations of cloud microphysics, turbulence and radiation must be such that they are applicable to a wide range of resolution. When it is successfully implemented, the practical merits of the unified parameterization will be great. But, we should remember that it has a limit as a "parameterization", which requires a number of idealizations to reduce the degrees of freedom. When sufficient computer resources are available, therefore, we should pursue the other approach, ROUTE II, for more realistic numerical weather prediction and climate simulations as discussed in the next section.

5. ROUTE II for the unification — the quasi-3D multiscale modeling framework

This section reviews ROUTE II for the unification following Jung and Arakawa (2010).

5.1. An overview of the MMF approach

In contrast to Route I, Route II attempts to use the CRM physics regardless of the GCM resolution. This is done through combining two grids, one for the GCM and the other for the CRM, and replacing the cloud parameterization in the GCM by the statistics of cloud processes simulated by the CRM. The prototype of this approach is "Cloud Resolving Convective Parameterization (CRCP)" (Grabowski and Smolarkiewicz, 1999; Grabowski, 2001), which is also called "Super-parameterization" (Khairoutdinov and Randall, 2001; Randall et al., 2003) or "Multiscale Modeling Framework (MMF)" (Khairoutdinov et al., 2008; Tao et al., 2009). To simulate cloud processes, the prototype MMF uses a 2D (horizontally 1D) CRM embedded in each GCM grid cell as schematically shown in Fig. 17(a). It can still be called a "parameterization" because the GCM recognizes only the domain-averaged values of the CRM results.

In the field of applied mathematics, various new methods of multiscale modeling have been developed, which use a microscopic model to obtain macroscopic information. Notable examples are the Heterogeneous Multi-scale Modeling (HMM) (E and Engquist, 2003; E et al., 2007, 2009) and the Equation-Free approach (Gear and Kevrekidis, 2003; Kevrekidis et al., 2003; Li et al., 2007). MMF is similar to the Equation-Free approach because the equations for cumulus parameterization in the GCM are completely replaced by the statistics of the CRM solution. There are important differences, however. The multiscale methods mentioned above critically depend on the existence of large spectral gaps both in space and time so that the microscopic model can be solved on small spatial-temporal domains. The use of a small temporal domain effectively assumes that the time scale for the macroscopic features of microscopic solutions to reach a quasi-equilibrium is much shorter than the macroscopic time scale. Based on this assumption, these methods (except E et al., 2009) reinitialize the microscopic model at every macroscopic time step. As we have seen in Section 2, the quasi-equilibrium of moist-convective process is a reasonable closure for the classical objective of cumulus parameterization. The objective of MMF is, however, to go beyond the quasi-equilibrium, which is especially important for unification of GCMs and CRMs. Thus, instead of using small temporal domains, the CRM component of MMF runs in parallel to the GCM component without gaps in time. Also, if a small spatial domain is used for the CRM component as in the multiscale methods, the possibility of simulating mesoscales may be completely lost. In contrast, the computing

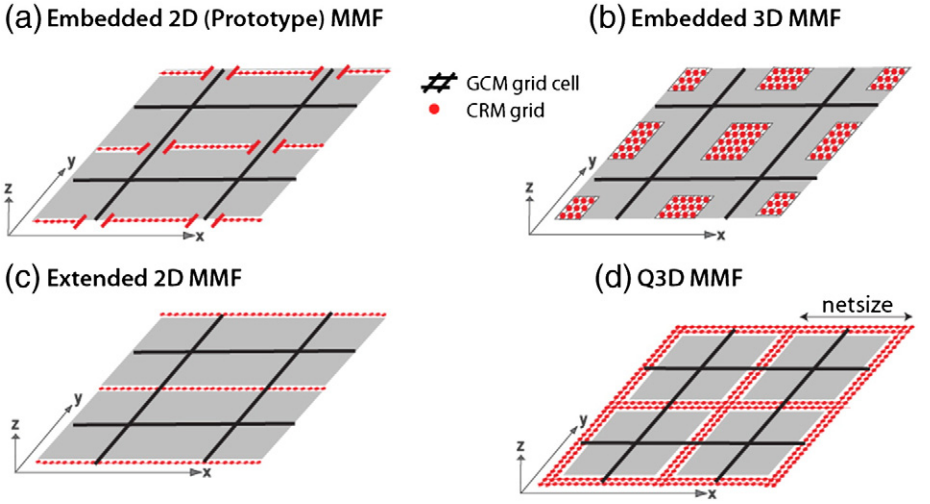

Fig. 17. Schematic illustration of the horizontal grid structures of (a) embedded 2D MMF, (b) embedded 3D MMF, (c) extended 2D MMF, and (d) Q3D MMF. The shaded areas represent gaps of the grid network.
Redrawn from JA10, their Fig. 5.

efficiency of MMF is gained through sacrificing full representation of cloud-scale 3D processes (except for the embedded 3D MMF described below). This is motivated by the fact that 2D CRMs are reasonably successful in simulating the gross thermodynamic effects of deep moist convection (e.g., Tao et al., 1987; Grabowski et al., 1998; Xu et al., 2002).

The prototype MMF has been evaluated (e.g., Ovtchinnikov et al., 2006; Khairoutdinov et al., 2008; Tao et al., 2009) and shown to improve climate simulations, including simulations of the Madden–Julian Oscillation (Benedict and Randall, 2009), low-cloud feedback on climate change (Wyant et al., 2009), and simulation of the coupled ocean–atmosphere system (Stan et al., 2010). While the performance of the prototype MMF presented in these papers is promising, it has the following inherent limits:

(i) The CRM component completely neglects three-dimensionality, while the circulation associated with clouds is three-dimensional especially when the background flow has vertical shear;
(ii) The CRM must a priori choose a particular direction for its orientation while the background flow predicted by the GCM component can be in any direction;
(iii) Each CRM is embedded within a GCM grid cell, and thus CRMs in neighboring GCM grid cells can communicate only indirectly through the GCM.

There have been variations of the prototype MMF. One is "Embedded 3D MMF" (Fig. 17(b)), in which the 2D CRM in the prototype MMF is replaced by a tiny 3D CRM (Khairoutdinov et al., 2005). With this, (i) and (ii) listed above are eliminated, but (iii) still remains. Moreover, to obtain computing efficiency comparable to the prototype MMF, the size of the 3D CRM is made very small, leaving practically no room for the mesoscale organization of clouds. Another variation is "Extended 2D MMF" (Fig. 17(c)). Here, the grid-point array of the 2D CRM is extended beyond the GCM grid cell without using a periodic boundary condition. Thus, (iii) is eliminated while (i) and (ii) still remain. Jung and Arakawa (2005) presented comparisons of the embedded and extended MMF simulations and showed that the extended MMF reduces systematic errors appeared in the embedded MMF simulation.

The quasi-3D (Q3D) MMF developed by Jung and Arakawa (2010, hereafter JA10) is an attempt to broaden the applicability of the prototype MMF without necessarily using a fully three-dimensional CRM. The main merit of the Q3D MMF is that it can converge to a 3D global CRM as the resolution of the GCM approaches that of the CRM. Consequently, the Q3D MMF can be applicable to any resolution of the GCM down to that of the CRM without changing the formulation of model physics and therefore the Q3D MMF and 3D CRM form a single family of models. The design of the Q3D MMF and its preliminary results of JA10 are presented in the next subsections.

5.2. The Q3D algorithm

The Q3D MMF is a modeling framework in which a GCM is coupled with a Q3D CRM. The Q3D CRM developed by JA10 is based on the 3D anelastic vorticity equation model of Jung and Arakawa (2008) applied to a horizontal domain with large gaps as illustrated in Fig. 17(d). Since the model is based on the anelastic system of equations, sound waves are filtered at their origin. In addition, the explicit representation of the 3D vorticity dynamics makes the computational design more straightforward because the pressure gradient force is eliminated.

As in the original 3D model, the Q3D CRM predicts the horizontal components of the vorticity. The vertical component is diagnostically determined by the vertical integration of the non-divergence condition of the 3D vorticity vector. To implement the anelastic approximation, the vertical velocity is determined from the predicted horizontal components of vorticity by solving an elliptic equation. JA10 uses a relaxation procedure for solving this equation by converting it to a parabolic equation, which formally predicts the vertical velocity (for details of this procedure, see JA10). The horizontal velocity components are then diagnostically determined from the known distributions of the horizontal components of vorticity and vertical velocity. Potential temperature and mixing ratios of various phases of water are also predicted. The physical parameterizations in the model include a three-phase microphysical parameterization (Lin et al., 1983; Lord et al., 1984; Krueger et al., 1995), a radiative transfer parameterization (Fu et al., 1995), a surface flux parameterization (Deardorff, 1972), and a first-order turbulence closure that uses eddy viscosity and diffusivity coefficients depending on deformation and stability (Shutts and Gray, 1994).

The horizontal domain of the Q3D CRM is illustrated in Fig. 18. The shaded areas in the figure indicate gaps where no prediction is made by the CRM. The gap size can be made smaller by one of the following two ways or their combinations: the first is by making the width of the channels thicker while using the same netsize as shown in Fig. 18(b). The second is by making the netsize smaller while staying with the same channel width as shown in Fig. 18(c). For computing efficiency, however, a large gap is preferred as shown in Fig. 18(a). Having only two grid points in the lateral direction of each channel is barely sufficient to accommodate active convective clouds of a typical size and to represent the twisting and stretching effects on vorticity in a non-trivial way.

To avoid singularity at the intersections, perpendicular channels of Q3D CRM are coupled only through mutual relaxations of the potential temperature and water vapor mixing ratio averaged over a segment of each channel centered at the intersection. This coupling is intended to mimic spreading of the warming and drying effects due to propagation of cumulus-induced internal gravity waves. Since this way of coupling is rather loose, individual channels perform almost independent simulations and, therefore, the self-stabilizing effect of convective activity is maintained in each channel without being overly constrained by the other channels. Especially when the mean flow has a vertical shear, these perpendicular channels can generate quite different statistics of simulated convective activity. However, as shown in the next subsection, the averages of the statistics simulated by these channels are very similar to the statistics generated by the 3D CRM. The Q3D network is further coupled with a GCM grid to form a Q3D MMF. It is mainly through this coupling that neighboring parallel channels can communicate with each other. The communication is generally statistical

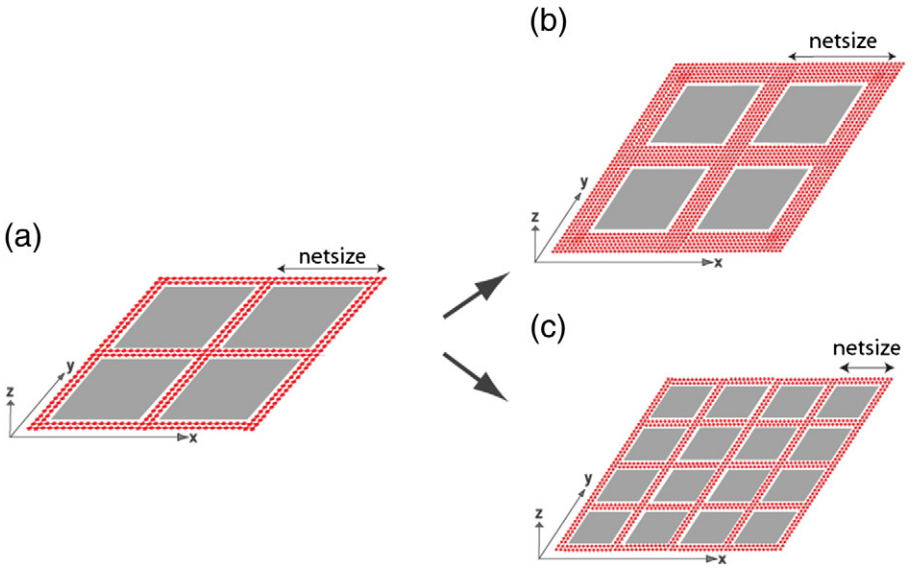

Fig. 18. Horizontal domains of the Q3D CRM with (a) a narrow channel width, (b) a widened channel width and (c) a reduced net size with a narrow channel width.
Redrawn from JA10, their Fig. 6.

but becomes more local as the GCM grid size approaches the CRM grid size.

An example of the horizontal distribution of prognostic variables in a portion of an x-channel is shown in Fig. 19. Following the original 3D CRM, grid points for the horizontal components of vorticity are staggered. The staggering shown in the figure makes the implementation of the non-divergence condition for vorticity most straightforward. As shown in the figure, there are two grid points for all prognostic variables in the lateral direction. With this choice, it is guaranteed that the degrees of freedom are balanced between the variables. If there is an imbalance in the degrees of freedom, it can cause an almost immediate instability of the solution in time integration.

The prediction algorithm of Q3D CRM is basically that of limited area modeling applied to the network of channels.

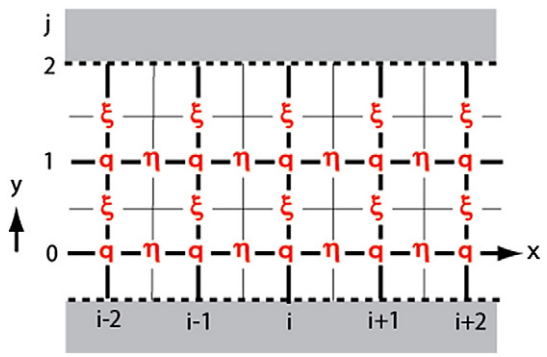

Fig. 19. Horizontal grid used in a channel of the Q3D CRM. Here, q is a scalar prognostic variable and ξ and η are vorticity components, respectively.
Taken from JA10, their Fig. 8.

However, due to the use of extremely narrow channels, the design of the lateral boundary condition is much more demanding than usual. For the purpose of designing the lateral boundary condition, the prognostic variables are assigned to the points located immediately outside the channel, q at $j=2$ in Fig. 19 for example, which are called "ghost points". Each field of the Q3D CRM is then separated into the background and deviation fields. The background field is obtained by interpolation of the GCM variables to each CRM point, including ghost points. The use of the background field determined in this way is one of the important features of the Q3D MMF because it allows the Q3D CRM to recognize the large-scale fields beyond the width of the narrow channel.

To determine the deviation field at ghost points, two requirements are imposed: 1) ghost point values should not cause computational instability, and 2) they should not significantly distort the statistics of internal solutions. The first requirement is the most fundamental requirement for the Q3D CRM to work. The second requirement is also important because the role of the CRM component of the MMF is to produce statistics of cloud scale processes. For advection, ghost-point values can be freely chosen in principle at inflow points. But if these values are too smooth, the variance of the internal solution tends to decrease. More generally, it is important for the ghost-point values at inflow points to have a probability density function (PDF) and spatial and temporal coherences similar to those of the internal solution. An easy way of fulfilling this is to borrow the values from the internal points. Through examining the normal-mode solutions of 1D advection equation with ghost-point values assigned by various linear combinations of the internal values, JA10 shows that the most effective way to satisfy these requirements is to use the periodic lateral boundary condition. Based on this result, the periodicity condition is chosen as the basis of designing the lateral boundary condition for the deviations of all variables of the model.

Convergence to a 3D CRM as the GCM grid size approaches the CRM grid size is one of the most important requirements for the Q3D MMF. An obvious necessary condition for the convergence is that the GCM and CRM components share the same dynamical core. Another obvious necessary condition is that the horizontal domain of the Q3D CRM occupies the entire domain in this limit. These two conditions are not sufficient for the convergence, however, because the gaps of the Q3D domain still exist although they shrink to points. This is because neighboring parallel channels do not directly communicate with each other due to the use of imposed lateral boundary conditions. To overcome this problem, the lateral boundary condition is applied only to the deviation from the background field. In addition, the CRM values are nudged to the interpolated GCM values more strongly as the grid size of GCM becomes close to that of the CRM. In this way, it is guaranteed that the deviation vanishes in that limit and thus the solution of the Q3D MMF is not affected by the imposed lateral boundary condition. Once the convergence is guaranteed, the Q3D MMF and 3D CRMs become a single family of models.

5.3. Preliminary results of the Q3D algorithm

To evaluate the Q3D algorithm in an efficient way, JA10 performed idealized experiments using a small horizontal domain (384 km × 384 km) with a grid size of 3 km. Two benchmark (BM) simulations are first made using a fully 3D CRM for typical tropical conditions with and without background wind shear. Fig. 20 shows examples of cloud development taken from the benchmark simulations. In the figure, snapshots of an isotomic surface ($=0.2\ \mathrm{g\ kg^{-1}}$) of the sum of cloud water and ice mixing ratios are shown for a selected time. With the background wind shear (BM1), organized cloud systems develop roughly in the direction normal to the low level shear, while small-scale convections more or less randomly develop without the background wind shear (BM2). This characteristic difference in the development of clouds between BM1 and BM2 remains throughout the simulation period.

In parallel to BM1 and BM2, two Q3D simulations are performed. Fig. 21(a) and (b) show the horizontal grids used for the BM and Q3D simulations, respectively. With the domain and grid sizes used, the ratio of the number of grid points of the Q3D and 3D CRMs is only 3%. Since the Q3D network consists of only a small portion of the 3D grid, the validity of using the Q3D network can be questioned from the point of view of sampling error. Fig. 21(c) shows the time series of surface precipitation rate obtained from BM1 averaged over the all grid points (black) and only over the Q3D grid points (blue). It can be seen that the time-average of the latter is quite close to the former although the latter strongly fluctuates in time due to the smaller sample size. Based on this finding, the network averages of Q3D simulations are compared with the domain averages of the BMs.

Each of the Q3D simulations takes initial conditions from $t=48$ hr of the corresponding BM. Since the horizontal domain is so small, the GCM component is made inactive and the values at GCM grid points are taken from the benchmark simulations with horizontal smoothing. These values are then interpolated to provide the background field for the Q3D CRM. Fig. 22 shows the time series of latent heat and sensible heat fluxes at the surface, obtained from the BM and Q3D simulations. These are averaged over their respective horizontal domains. As expected, the Q3D results fluctuate more than those of the BM but their amplitudes are significantly smaller than those shown in Fig. 21(c) because the dynamics of the Q3D CRM is closed even with the grid shown in Fig. 21(b). The time averages of the Q3D fluxes are quite close to corresponding fluxes of the BM, indicating that the Q3D CRM is able to capture the characteristics of two different cloud regimes at least qualitatively.

In the following, selected results from the BM1 case are presented. Fig. 23 shows vertical profiles of the time- and

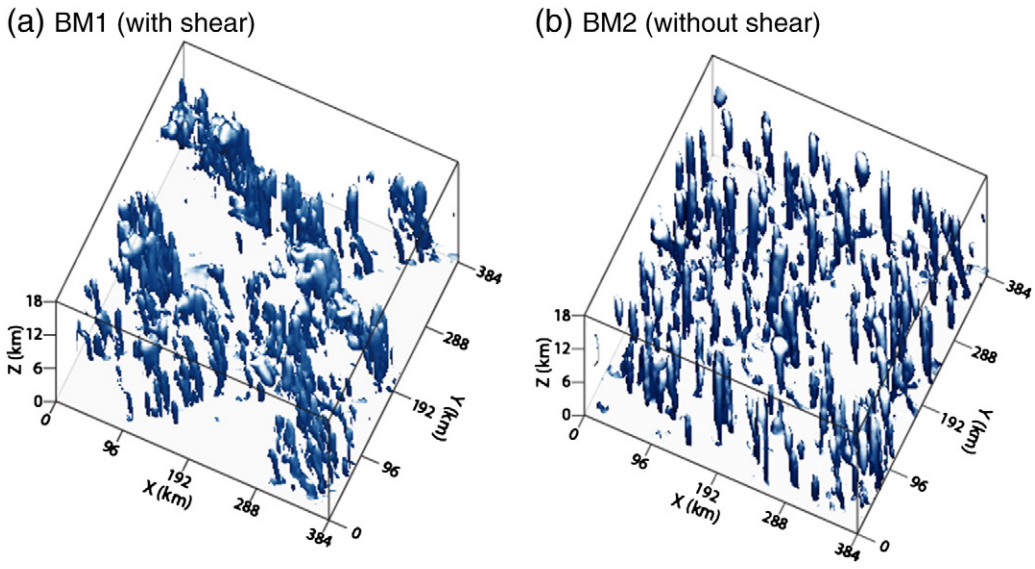

Fig . 20. Snapshots of an isotomic surface ($=0.2\ \mathrm{g\ kg^{-1}}$) of the sum of cloud water and ice mixing ratios obtained from (a) BM1 and (b) BM2. Taken from JA10, their Fig. 11.

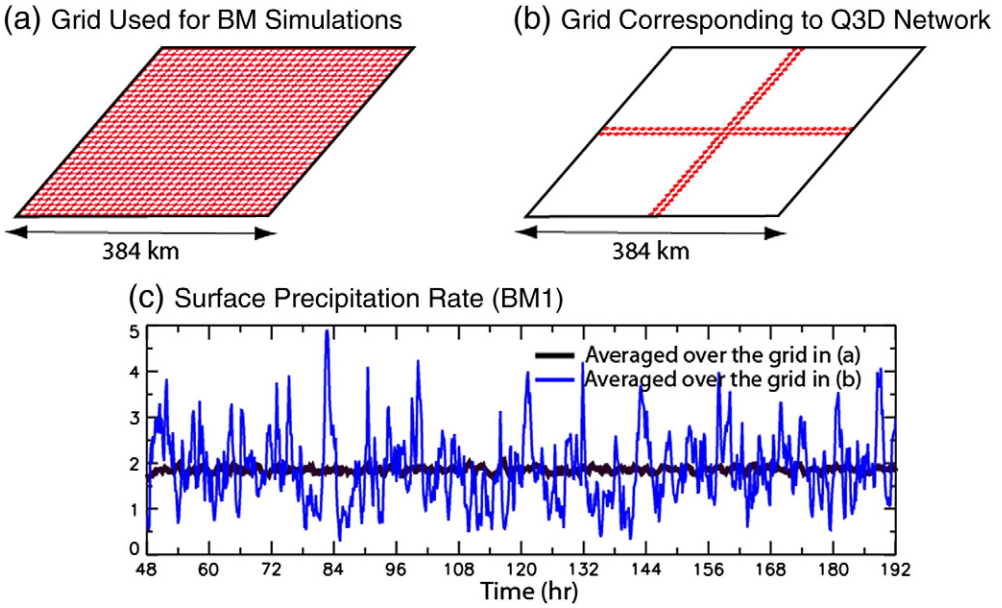

Fig. 21. Schematic illustration of (a) the grid used for BM simulations and (b) grid corresponding to the Q3D network and (c) time series of the surface precipitation rates obtained from BM1. Here, black and blue lines represent the precipitation rates averaged over the grids in (a) and (b), respectively.
Taken from JA10, their Fig. 12.

domain-averaged vertical transports of potential temperature, water vapor mixing ratio, and the horizontal components of vorticity. The vertical transport of potential temperature, which is a measure of the buoyancy generation of kinetic energy, is slightly under-predicted by the Q3D. On the other hand, the vertical transport of water vapor shows an almost perfect agreement with BM1. The transports of vorticity components are also well simulated in the Q3D runs. It indicates that the Q3D CRM simulates the cloud-scale 3D processes reasonably well in spite of the use of the highly limited number of grid points across the channels.

Based on the comparisons of the simulated results with those of BM simulations, JA10 concluded that the Q3D algorithm is quite successful especially in simulating the case where clouds are well organized into a squall-line type structure. Having two perpendicular sets of channels enables the CRM component to recognize the orientation of the organized cloud system reasonably well. It is less successful, however, for the case where small clouds are scattered with an almost purely three-dimensional structure. For better representation of scattered clouds in the Q3D MMF, an inclusion of a stochastic component seems to be needed.

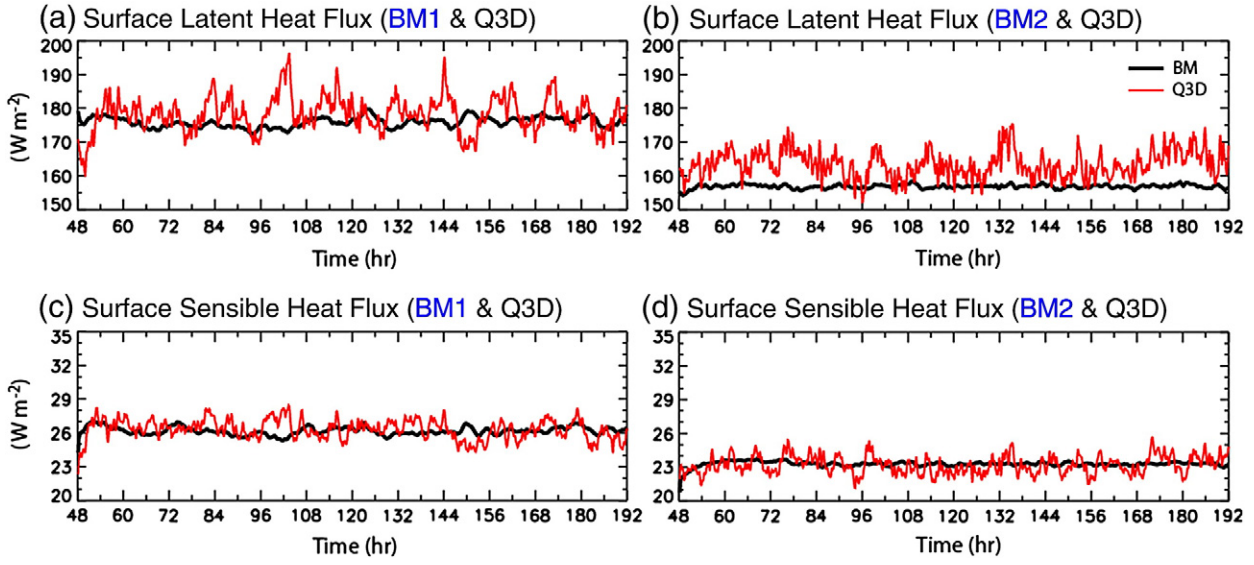

Fig. 22. Time series of the [(a) and (b)] surface latent heat and [(c) and (d)] sensible heat fluxes averaged over the respective horizontal domain. Here, (a) and (c) are obtained from the BM1 case and (b) and (d) from the BM2 case. Black and red lines represent BM and Q3D simulations, respectively.
Redrawn from JA10, their Fig. 13.

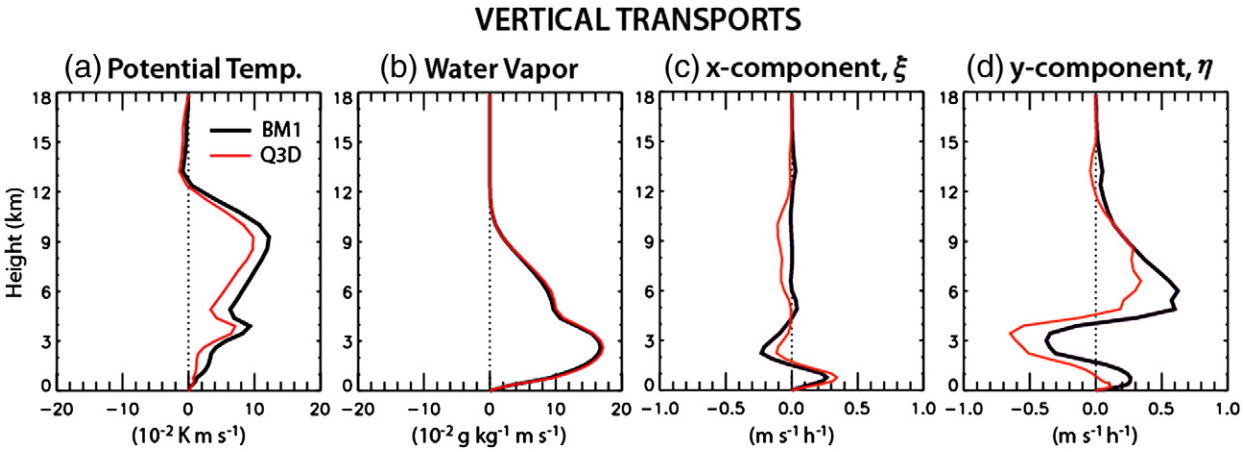

Fig. 23. Time- and domain-averaged profiles of the vertical transports of (a) potential temperature, (b) water vapor, and (c) *x*- and (d) *y*-components of vorticity. Redrawn from JA10, their Figs. 19 and 20.

Similar comparisons are made between the Q3D CRM and the corresponding two 2D simulations, one placed along the *x*-direction and the other along the *y*-direction. When this 2D CRM is coupled with a GCM component, the framework is equivalent to that of the extended 2D MMF shown in Fig. 17(c). The statistics of the two 2D simulations are quite different from each other and thus the results of the two 2D simulations are averaged to compare with the Q3D results. Significant improvements in the Q3D simulation compared to the corresponding 2D simulations appear especially in the surface fluxes (Fig. 24) and the vertical vorticity transports (Fig. 25). These improvements are expected because the surface fluxes depend on the two components of surface horizontal wind and the dynamical interactions between convection and the mean flow are inherently three-dimensional.

Comparisons between the simulations of BM1, Q3D and coarse-resolution 3D show that the low-level cloud water is over-predicted and the surface latent heat flux is under-predicted with the coarse 3D CRM as shown in Fig. 26. This is probably due to the inefficient upward transport of moisture with the coarse-resolution. Most of the statistical properties of deep convective activity are, however, reasonably reproduced by the coarse 3D CRM that has a computing efficiency comparable to that of the Q3D CRM (e.g., Fig. 27). This is presumably because the same large-scale thermal forcing is prescribed in these experiments regardless of the resolution. Further assessment of the resolution dependency, however, should be made with a larger horizontal domain that allows the model to produce its own large-scale forcing.

For large-scale applications, the Q3D network is coupled with a GCM grid. Coupling the dynamics of the two models is important especially in view of the convergence of the Q3D MMF to a 3D CRM. In the prototype MMF, the coupling strategy is such that the effect of large-scale processes is given to the CRM component in the form of forcing and the

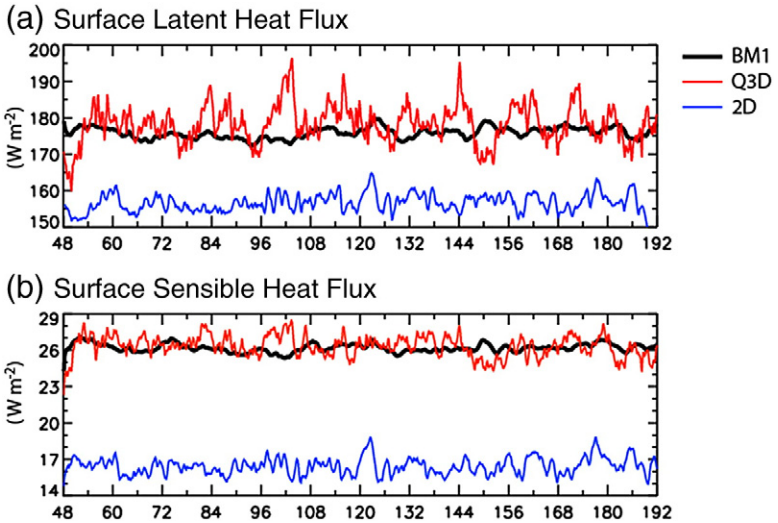

Fig. 24. Time series of the surface fluxes of (a) latent heat and (b) sensible heat. Redrawn from JA10, their Fig. 21.

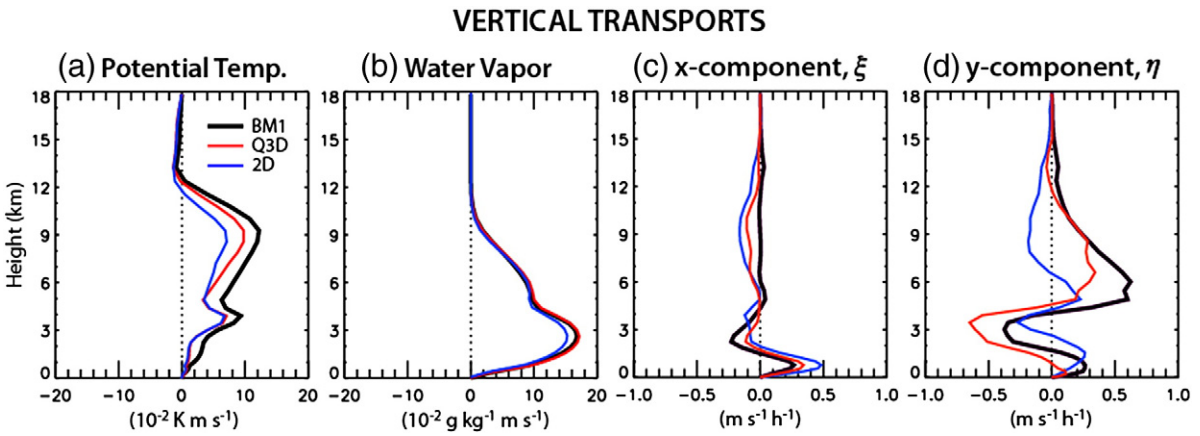

Fig. 25. As in Fig. 23, but from BM1, Q3D, and 2D simulations.
Redrawn from JA10, their Fig. 23.

large-scale fields are adjusted to the horizontal average of the cloud scale effects simulated by the CRM (Grabowski and Smolarkiewicz, 1999). No momentum feedback is included, however, in the recent applications of the MMF (Khairoutdinov et al., 2008; Tao et al., 2009). In the Q3D MMF, the Q3D CRM grid extends beyond the GCM grid cell so that it can represent large-scale processes at least partially. If the coupling strategy of the prototype MMF is directly followed in the Q3D MMF, the problem of "double counting" of large-scale processes is inevitable. Our solution for this problem is briefly outlined in Section 6 and will be discussed further in our forthcoming paper.

6. Summary and conclusion

The importance of multiscale modeling of moist-convective atmosphere was recognized in the early 1960s in tropical cyclone modeling when the idea of CISK was introduced. In CISK, cyclone-scale and moist-convective scale of motion cooperate with each other for simultaneous development in a conditionally unstable atmosphere. Although this idea became popular among the tropical meteorology community, its physical basis can be questioned. An alternative idea for multiscale modeling of moist-convective atmosphere is moist-convective adjustment of the conditionally unstable environment to a neutral state. This idea was introduced first in general circulation modeling also in the 1960s. If the adjustment takes place sufficiently fast compared to the destabilization of the environment by other processes, we expect that the atmosphere undergo a sequence of quasi-neutral states in which large-scale destabilization and moist-convective stabilization approximately balance. This leads to the concept of moist-convective quasi-equilibrium as reviewed in Section 2. It seems that many existing cumulus parameterizations use this kind of closure typically with a finite time scale for adjustment. To a large extent, the history of cumulus parameterization has been designing, revising, evaluating and tuning of closure assumptions, cloud models, and formulations of convective triggering. Practically all of these efforts are, however, based on the modular structure shown in Fig. 3, which can be justified only when there is a spectral gap both in space and time. It is pointed out that the history has reached the stage at which we should seriously question the impact of this artificial separation.

Strictly speaking, truncation of a continuous system can be justified only when the resulting error can be made arbitrarily

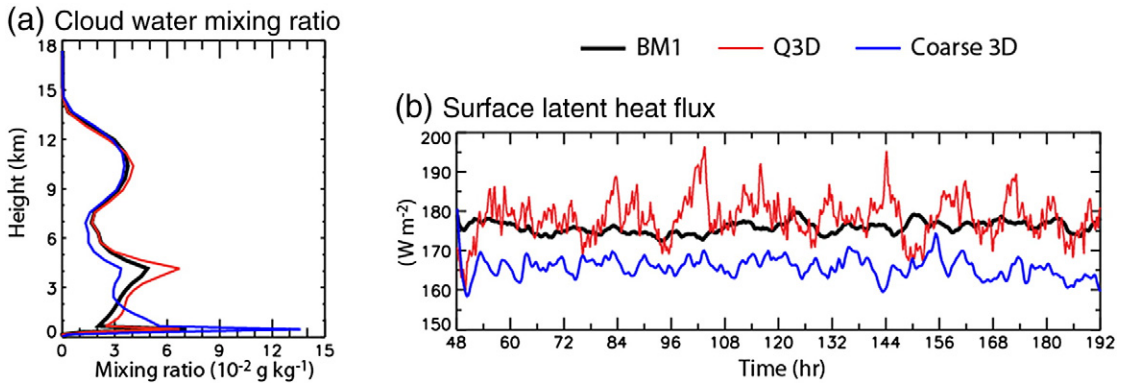

Fig. 26. (a) Time- and domain-averaged profile of the sum of cloud liquid and ice water mixing ratios, and (b) time series of the surface latent heat flux obtained from BM1, Q3D, and coarse 3D simulations.
Redrawn from JA10, their Figs. 24 and 25.

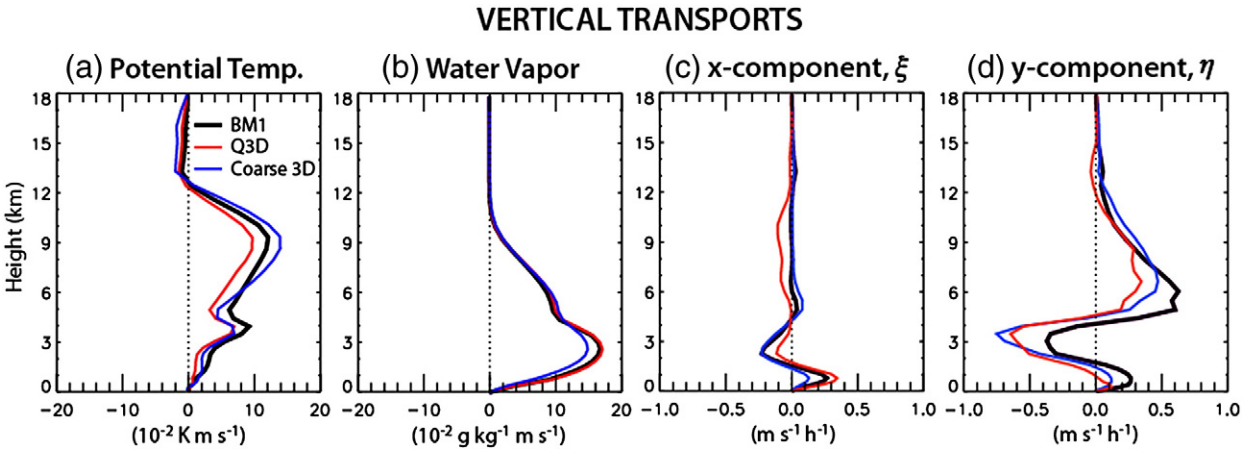

Fig. 27. As in Fig. 23, but from BM1, Q3D, and coarse 3D simulations. Redrawn from JA10, their Fig. 26.

small by using a higher resolution. This requires that the dynamics and physics of the low-resolution models converge to those of the high-resolution models with an increase of the horizontal resolution. Unfortunately, this is not the case for the conventional formulations of model physics in GCMs because it is not based on a sufficiently general framework for representing the multiscale effects of moist-convective processes. If the model physics of GCMs is reformulated in such a way that it converges to that of CRMs, these two kinds of model physics are unified. Then, we can freely choose intermediate resolutions or highly heterogeneous resolutions such as in the local or adaptive mesh refinement while staying with the same formulation of model physics.

This paper reviews two possible routes to achieve the unification. ROUTE I uses a new framework for cumulus parameterization in which the result of parameterization converges to an explicit simulation of cloud processes as the resolution increases. In this way the framework unifies parameterizations in GCMs and CRMs as far as the representation of deep moist convection is concerned. With the unified parameterization, the error of the GCM solution to satisfy the CRM equations can be made arbitrarily small by using a higher resolution. It is shown that a key to construct a unified parameterization is to eliminate the assumption of small fractional area covered by convective clouds, which is commonly assumed in the conventional cumulus parameterizations either explicitly or implicitly. A preliminary design of the unified parameterization is presented and partially evaluated, which demonstrates that such an assumption could be eliminated through a relatively minor modification of the existing mass-flux based parameterizations. It is also shown that the unified parameterization provides a physical and quantitative basis for the relaxed adjustment that gives a more room for explicit simulations of the transports.

There are two main sources for uncertainty in the results of the unified parameterization: one is the non-deterministic nature of the closure and the other is estimating cloud properties with huge dimensions by a simple cloud model that has only limited degrees of freedom. This may suggest the necessity of including a stochastic component in the parameterization. It should be noted, however, that such a component is not needed for large values of σ because the explicit simulation by the CRM can act as a random-process generator by itself. In what way and to what extent we should include the stochastic component in the unified parameterization is one of the remaining questions.

The unified parameterization has its own scientific merit because of its simple structure. When sufficient computer resources are available, however, we should rather pursue the other approach, ROUTE II, which follows the MMF approach to statistically couple GCM and CRM grids. The Quasi-3D (Q3D) MMF is an attempt to broaden the applicability of the prototype MMF without necessarily using a fully three-dimensional CRM. To overcome some of the limitations of the prototype MMF, such as the two-dimensionality and periodic boundary conditions of the embedded CRMs, the Q3D MMF introduces a horizontal domain that consists of two perpendicular sets of channels, each of which contains a locally 3D array of grid points. For computing efficiency, the widths of these channels are chosen to be narrow barely sufficient to accommodate active convective clouds of a typical size. Thus, when a relatively large grid size is used for the CRM component, the number of grid points in the lateral direction can be as small as two.

The algorithm of the Q3D CRM is basically that of limited area modeling applied to a horizontal domain with gaps. However, due to the use of narrow channels, the design of the lateral boundary condition is much more demanding than usual limited-area modeling. An obvious necessary requirement is that the lateral boundary condition should not cause computational instability. In addition, it must not significantly distort the statistics of internal solutions. Among the various possibilities examined, it is found that the most effective way to satisfy these requirements is to use the periodic lateral boundary condition for the deviations of all variables from their background values given by interpolation of the GCM variables.

A great advantage of the Q3D MMF is that, as in the unified parameterization, it converges to a 3D CRM as the GCM's resolution is refined while maintaining the same model physics. In the Q3D MMF, the model physics is the CRM physics throughout. An outline of the Q3D algorithm

and highlights of preliminary results are reviewed. Comparing the simulation results with the corresponding benchmark simulation performed with a 3D CRM, it is concluded that the Q3D CRM can reproduce most of the important statistics of the 3D solutions, including precipitation rate and heat fluxes at the surface and vertical profiles of the vertical transports of major prognostic variables. Significant improvements compared to the corresponding 2D simulations appear especially in the surface fluxes and the vertical vorticity transports. In the solution of a coarse-resolution 3D CRM that has approximately the same number of grid points with that of the Q3D CRM, the low-level moist static energy and cloud water are over-predicted and the surface latent heat flux is under-predicted. This is probably due to the inefficient upward transport of moisture with the coarse-resolution.

The Q3D algorithm is quite successful in simulating the case where clouds are well organized into a squall-line type. Idealized squall lines, which have a linear structure, are rather two-dimensional phenomena so that they can be more easily represented by the Q3D grid system if the system can recognize their orientation. Having two perpendicular sets of channels enables the CRM component to recognize the orientation reasonably well. It is less successful, however, for the case where small clouds are scattered and therefore cloud circulations are almost purely three-dimensional. It is not an easy task to successfully simulate the pure 3D case with a "gappy" grid system. To represent scattered clouds better in the Q3D MMF, a stochastic component may have to be included.

In the tests performed, the Q3D CRM is not interactively coupled with the GCM component because the horizontal domain is very small so that the GCM cannot produce any physically meaningful horizontal inhomogeneity. For large-scale applications, however, the Q3D network should be coupled with a GCM grid. Coupling the dynamics of the two models is important, especially in view of the convergence of the Q3D MMF to a 3D CRM. In the Q3D MMF, the CRM grid extends beyond the GCM grid cell so that it can represent large-scale dynamics and, therefore, the CRM can generate its own large-sale forcing. To avoid "double counting" of large-scale dynamic processes, we are planning to choose a way in which the Q3D CRM is responsible only for calculating the mean nonlinear effects of the deviations (e.g., eddy transport terms) and most of the diabatic effects due to sub-grid processes. The netsize-averages of the CRM prognostic variables are adjusted to the GCM prognostic variables, loosely/tightly when the GCM resolution is low/high. It is mainly through this coupling that neighboring parallel channels can communicate with each other. The communication is generally statistical but becomes more local as the GCM grid size approaches the CRM grid size.

The Q3D MMF and GCMs with the unified parameterization still represent different families of models although they converge to the same model, a GCRM, as the GCM resolution approaches the CRM resolution (see Fig. 28). We envision that the hierarchy of future global models should form a "Multiscale Modeling Network (MMN)", which combines the above two routes as shown by the vertical dashed line in Fig. 28. With this network, the horizontal resolution of the dynamics core and that of the physical processes can be individually and freely chosen anywhere between those of the conventional GCMs and CRMs without changing the formulation of model physics.

Fig. 29 illustrates the history of numerical modeling of the atmosphere. The period of 1950s, which can be characterized by "Victory of Simplification", began with the first successful numerical weather prediction (NWP) by Charney et al. (1950) using an equivalent-barotropic quasi-geostrophic model. The period from the 1960s through 2000s, which can be characterized by "Expansion of the Scope and Diversity", began with the development of the early GCMs. A number of numerical models are subsequently developed for different scales. From the 2000s to present, there is a tendency toward "Unification" of these models. The approaches of MMF and MMN reviewed in this paper expand the unification all the way from GCMs to CRMs as shown by the red bracket in the figure.

Acknowledgments

We wish to thank Professor David Randall for his interest and support of this work and for a number of useful

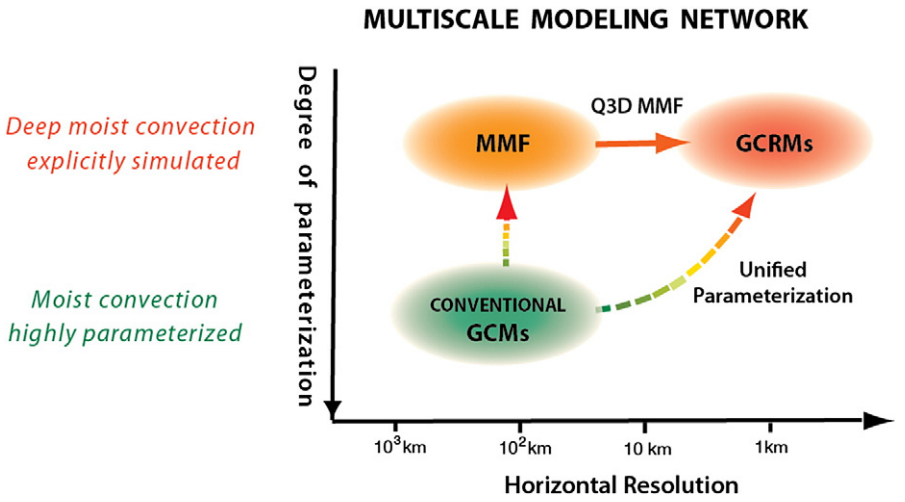

Fig. 28. Multiscale modeling network that consists of the unified parameterization, the Q3D MMF, and a link between the two.

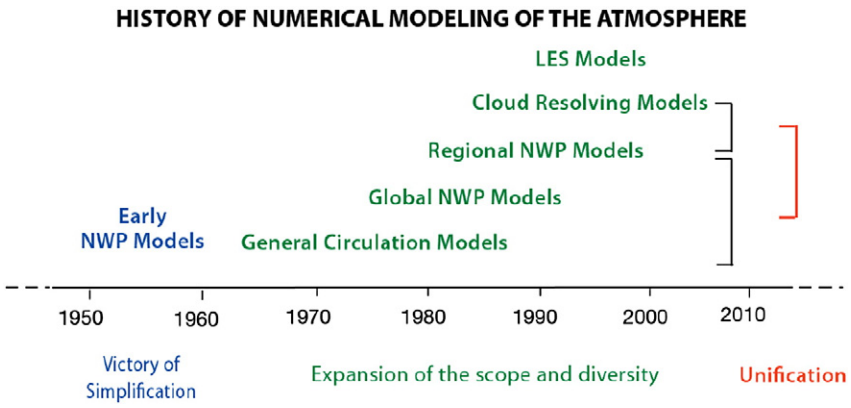

Fig. 29. Illustration of the history of numerical modeling of the atmosphere.

comments. We also thank Dr. Chien-Ming Wu for his analysis of simulated data included in Section 4. This research has been supported by the National Science Foundation Science and Technology Center for Multi-Scale Modeling of Atmospheric Processes, managed by Colorado State University under cooperative agreement No. ATM-0425247.

References

Arakawa, A., 1969. Parameterization of cumulus clouds. Proc. WMO/IUGG Symposium on Numerical Weather Prediction. Tokyo, IV, 8, pp. 1–6.
Arakawa, A., 1975. Modelling clouds and cloud processes for use in climate model. The Physical Basis of Climate and Climate Modelling (GARP Publication Series No. 16), pp. 183–197.
Arakawa, A., 1993. Closure assumptions in the cumulus parameterization problem. The Representation of Cumulus Convection in Numerical Models: Meteor. Monogr. Amer. Meteor. Soc., No. 46, pp. 1–16.
Arakawa, A., 2004. The cumulus parameterization problem: past, present, and future. J. Climate 17, 2493–2525.
Arakawa, A., Chen, J.-M., 1987. Closure assumptions in the cumulus parameterization problem. In: Matsuno, T. (Ed.), Short- and medium-range numerical prediction, collection of papers presented at the WMO/IUGG NWP symposium, Tokyo, 4–8 August 1986: Meteor. Soc. Japan, pp. 107–131.
Arakawa, A., Cheng, M.-D., 1993. The Arakawa–Schubert cumulus parameterization. In: Emanuel, K.A., Raymond, D.J. (Eds.), The representation of cumulus convection in numerical models of the atmosphere: American Meteorological Society, pp. 123–136.
Arakawa, A., Schubert, W.H., 1974. Interaction of a cumulus cloud ensemble with the large-scale environment. Part I. J. Atmos. Sci. 31, 674–701.
Arakawa, A., Jung, J.-H., Wu, C.-M., 2011. Toward unification of the multiscale modeling of the atmosphere. Atmos. Chem. Phys. 11, 3731–3742. doi:10.5194/acp-11-3731-2011.
Benedict, J.J., Randall, D.A., 2009. Structure of the Madden–Julian oscillation in the superparameterized CAM. J. Atmos. Sci. 66, 3277–3296. doi:10.1175/2009JAS3030.1.
Betts, A.K., 1986. A new convective adjustment scheme. Part I: observational and theoretical basis. Quart. J. R. Meteor. Soc. 112, 677–691.
Betts, A.K., Miller, M.J., 1986. A new convective adjustment scheme. Part II: single column tests using GATE wave. BOMEX, ATEX and arctic airmass data sets. Quart. J. R. Meteor. Soc. 112, 693–709.
Betts, A.K., Miller, M.J., 1993. The Betts–Miller scheme. The representation of cumulus convection in numerical models. Meteor. Monogr. Amer. Meteor. Soc. 46, 107–122.
Bjerknes, J., 1938. Saturated-adiabatic ascent of air through dry-adiabatically descending environment. Quart. J. Roy. Meteor. Soc. 64, 325–330.
Charney, J.G., Eliassen, A., 1964. On the growth of the hurricane depression. J. Atmos. Sci. 21, 68–75.
Charney, J.G., Fjørtoft, R., von Neumann, J., 1950. Numerical integration of the barotropic vorticity equation. Tellus 2, 237–254.
Deardorff, J.W., 1972. Parameterization of the planetary boundary layer for use in general circulation models. Mon. Wea. Rev. 100, 93–106.
E, W., Engquist, B., 2003. The heterogeneous multi-scale methods. Commun. Math. Sci. 1, 87–132.
E, W., Engquist, B., Li, X., Ren, W., Vanden-Eijnden, E., 2007. Heterogeneous multiscale methods: a review. Commun. Comput. Phys. 2, 367–450.
E, W., Ren, W., Vanden-Eijnden, E., 2009. A general strategy for designing seamless multiscale methods. J. Comp. Phys. 228, 5437–5453.
Emanuel, K.A., 1986. An air–sea interaction theory for tropical cyclones. Part I: steady-state maintenance. J. Atmos. Sci. 43, 585–604.
Emanuel, K.A., 1991. A scheme for representing cumulus convection in large-scale models. J. Atmos. Sci. 48, 2313–2335.
Emanuel, K.A., 1994. Atmospheric Convection. Oxford University Press, New York. 580 pp.
Emanuel, K.A., Raymond, D.J., 1992. Report from a workshop on cumulus parameterization, Key Biscayne, Florida, 3–5 May 1991. Bull. Amer. Meteor. Soc. 73, 318–325.
Emanuel, K.A., Neelin, J.D., Bretherton, C.S., 1994. On large-scale circulations in convecting atmosphere. Q. J. Roy. Meteor. Soc. 120, 1111–1143.
Frank, W.M., 1993. A hybrid parameterization with multiple closures. The representation of cumulus convection in numerical models. Meteor. Monogr. Amer. Meteor. Soc. 46, 151–154.
Fu, Q., Krueger, S.K., Liou, K.N., 1995. Interactions of radiation and convection in simulated tropical cloud clusters. J. Atmos. Sci. 52, 1310–1328.
Gear, C.W., Kevrekidis, I.G., 2003. Projective methods for stiff differential equations: problems with gaps in their eigenvalue spectrum. SIAM J. Sci. Comput. 24, 1091–1106.
Grabowski, W.W., 2001. Coupling cloud processes with the large-scale dynamics using the cloud-resolving convective parameterization (CRCP). J. Atmos. Sci. 58, 978–997.
Grabowski, W.W., Smolarkiewicz, P.K., 1999. CRCP: a cloud resolving convective parameterization for modeling the tropical convective atmosphere. Physica D 133, 171–178.
Grabowski, W.W., Wu, X., Moncrieff, M.W., Hall, W.D., 1998. Cloud-resolving modeling of cloud systems during Phase III of GATE. Part II: effects of resolution and the third spatial dimension. J. Atmos. Sci. 55, 3264–3282.
Gregory, D., Rowntree, P.R., 1990. A mass flux convection scheme with representation of cloud ensemble characteristics and stability dependent closure. Mon. Wea. Rev. 118, 1483–1506.
Jung, J.-H., Arakawa, A., 2004. The resolution dependence of model physics: illustrations from nonhydrostatic model experiments. J. Atmos. Sci. 61, 88–102.
Jung, J.-H., Arakawa, Akio, 2005. Preliminary tests of multiscale modeling with a two-dimensional framework: sensitivity to coupling methods. Mon. Wea. Rev. 133, 649–662.
Jung, J.-H., Arakawa, A., 2008. A three-dimensional anelastic model based on the vorticity equation. Mon. Wea. Rev. 135, 276–294. doi:10.1175/2007MWR2095.1.
Jung, J.-H., Arakawa, A., 2010. Development of a quasi-3d multiscale modeling framework: motivation, basic algorithm and preliminary results. J. Adv. Model. Earth Syst. 2. doi:10.3894/JAMES.2010.2.11 Art. #11, 31 pp.
Kain, J.S., Fritsch, J.M., 1990. A one-dimensional entraining/detraining plume model and its application in convective parameterization. J. Atmos. Sci. 47, 2784–2802.
Kain, J.S., Fritsch, J.M., 1993. Convective parameterization for mesoscale models: the Kain–Fritsch scheme. The representation of cumulus convection in numerical models. Meteor. Monogr. Amer. Meteor. Soc. 46, 165–170.
Kain, J.S., Fritsch, J.M., 1998. Multiscale convective overturning in mesoscale convective systems: reconciling observations, simulations, and theory. Mon. Wea. Rev. 126, 2254–2273.

Kasahara, A., 1962. The development of forced convection caused by the released latent heat of condensation in a hydrostatic atmosphere. Proc. International Symposium on Numerical Weather Prediction., Tokyo, Nov. 1960. Meteor, Soc. Japan, pp. 387–403.
Kasahara, A., 2000. On the origin of cumulus parameterization for numerical prediction models. In: Randall, D.A. (Ed.), General Circulation Model Development: Past, Present, and Future. Academic Press, pp. 199–224.
Kevrekidis, I.G., Gear, C.W., Hyman, J.M., Kevrekidis, P.G., Runborg, O., Theodoropoulos, C., 2003. Equation-free multiscale computation: enabling microscopic simulators to perform system-level tasks. Commun. Math. Sci. 1 (2003), 715–762.
Khairoutdinov, M.F., Randall, D.A., 2001. A cloud-resolving model as a cloud parameterization in the NCAR community climate system model: preliminary results. Geophys. Res. Lett. 28, 3617–3620.
Khairoutdinov, M.F., Randall, D.A., DeMott, C., 2005. Simulations of the atmospheric general circulation using a cloud-resolving model as a superparameterization of physical processes. J. Atmos. Sci. 62, 2136–2154.
Khairoutdinov, M.F., DeMott, C., Randall, D.A., 2008. Evaluation of the simulated interannual and subseasonal variability in an AMIP-style simulation using the CSU multiscale modeling framework. J. Climate 21, 413–431. doi:10.1175/2007JCL11630.1.
Krueger, S.K., 2002. Current issues in cumulus parameterization. ECMWF Seminar on Key Issues in the Parameterization of Subgrid Physical Processes, ECMWF, Reading, 3–7 September 2001, pp. 25–51.
Krueger, S.K., Luo, Y., 2004. Grid-size dependence of cumulus parameterization. Extended Abstracts, 20th Conference on Weather Analysis and Forecasting/16th Conference on Numerical Weather Prediction, Seattle, WA, Amer. Meteor. Soc.
Krueger, S.K., Fu, Q., Liou, K.N., Chin, H.-N., 1995. Improvements of an ice-phase microphysics parameterization for use in numerical simulations of tropical convection. J. Appl. Meteor. 34, 281–287.
Kuo, H.L., 1974. Further studies of the parameterization of the influence of cumulus convection on large-scale flow. J. Atmos. Sci. 31, 1232–1240.
Li, J., Kevrekidis, P.G., Gear, C.W., Kevrekidis, I.G., 2007. Deciding the nature of the coarse equation through microscopic simulations: the baby–bathwater scheme. SIAM Rev. 49 (3), 469–487.
Lilly, D.K., 1960. On the theory of disturbances in the conditionally unstable atmosphere. Mon. Wea. Rev. 88, 1–17.
Lin, Y.-L., Farley, R.D., Orville, H.D., 1983. Bulk parameterization of the snow field in a cloud model. J. Climate. Appl. Meteor. 22, 1065–1092.
Lord, S.J., Arakawa, A., 1980. Interaction of a cumulus cloud ensemble with the large-scale environment. Part II. J. Atmos. Sci. 37, 2677–2692.
Lord, S.J., Willoughby, H.E., Piotrowicz, J.M., 1984. Role of a parameterized ice-phase microphysics in an axisymmetric, nonhydrostatic tropical cyclone model. J. Atmos. Sci. 41, 2836–2848.
Manabe, S., Smagorinsky, J., Strickler, R.F., 1965. Simulated climatology of a general circulation model with a hydrological cycle. Mon. Wea. Rev. 93, 769–798.
Mintz, Y., 1958. Design of some numerical general circulation experiments. Bull. Res. Counc. Isr., Geosci. 7G, 67–114 (ADD).
Molinari, J., 1993. An overview of cumulus parameterization in mesoscale models. The representation of cumulus convection in numerical models. Meteor. Monogr. Amer. Meteor. Soc. 46, 155–158.
Molinari, J., Dudek, M., 1992. Parameterization of convective precipitation in mesoscale numerical models: a critical review. Mon. Wea. Rev. 120, 326–344.
Moorthi, S., Suarez, M.J., 1992. Relaxed Arakawa–Schubert: a parameterization of moist convection for general circulation models. Mon. Wea. Rev. 120, 978–1002.
Ooyama, K., 1964. A dynamical model for the study of tropical cyclone development. Geofisica Internacional 4, 187–198.
Ooyama, K., 1969. Numerical simulation of the life cycle of tropical cyclones. J. Atmos. Sci. 26, 3–40.
Ovtchinnikov, M., Ackerman, T., Marchand, R., 2006. Evaluation of the multiscale modeling framework using the data from the atmospheric radiation measurement program. J. Climate 19, 1716–1729.
Randall, D.A., Ding, P., Pan, D.-M., 1997a. The Arakawa–Schubert cumulus parameterization. In: Smith, R.K. (Ed.), The Physics and Parameterization of Moist Atmospheric Convection. Kluwer Academic Publishers, pp. 281–296.
Randall, D.A., Pan, D.-M., Ding, P., Cripe, D.G., 1997b. Quasi-equilibrium. In: Smith, R.K. (Ed.), The Physics and Parameterization of Moist Atmospheric Convection. Kluwer Academic Publishers, pp. 359–386.
Randall, D.A., Khairoutdinov, M., Arakawa, A., Grabowski, W., 2003. Breaking the cloud parameterization deadlock. Bull. Amer. Meteor. Soc. 84, 1547–1564.
Raymond, D.J., Emanuel, K., 1993. The Kuo cumulus parameterization. The representation of cumulus convection in numerical models. Meteor. Monogr. Amer. Meteor. Soc. 46, 145–150.
Sato, T., Miura, H., Satoh, M., Takayabu, Y.N., Wang, Y., 2009. Diurnal cycle of precipitation in the tropics simulated in a global cloud-resolving model. J. Climate 22, 4809–4826. doi:10.1175/2009JCLI2890.1.
Shutts, G.J., Gray, M.E.B., 1994. A numerical modeling study of the geostrophic adjustment process following deep convection. Q. J. R. Meteor. Soc. 120, 1145–1178.
Smagorinsky, J., 1956. On the inclusion of moist-adiabatic processes in numerical prediction models. Ber. Dtsch. Wetterdienstes 5, 82–90.
Stan, C., Khairoutdinov, M., DeMott, C.A., Krishnamurthy, V., Straus, D.M., Randall, D.A., Kinter III, J.L., Shukla, J., 2010. An ocean–atmosphere climate simulation with an embedded cloud resolving model. Geophys. Res. Lett. 37, L01702. doi:10.1029/2009GL 040822.
Tao, W.-K., Simpson, J., Soong, S.-T., 1987. Statistical properties of a cloud ensemble: a numerical study. J. Atmos. Sci. 44, 3175–3187.
Tao, W.-K., Chern, J.-D., Atlas, R., Randall, D.A., Khairoutdinov, M., Li, J.-L.., Waliser, D.E., Hou, A., Lin, X., Peters-Lidard, C., Lau, W., Jiang, J., Simpson, J., 2009. A multiscale modeling system: developments, applications, and critical issues. Bull. Amer. Meteor. Soc. 90, 515–534. doi:10.1175/2008BAMS 2542.1.
Tiedtke, M., 1989. A comprehensive mass flux scheme for cumulus parameterization in large-scale models. Mon. Wea. Rev. 117, 1779–1800.
Williamson, D.L., 1999. Convergence of atmospheric simulations with increasing horizontal resolution and fixed forcing scales. Tellus 51A, 663–673.
Wyant, M.C., Bretherton, C.S., Blossey, P.N., 2009. Subtropical low cloud response to a warmer climate in a superparameterized climate model. Part I: regime sorting and physical mechanisms: J. Adv. Model. Earth Syst. . doi:10.3894/JAMES. 2009.1.7. 1, Art. #7, 11pp.
Xu, K.M., Cederwall, R.T., Donner, L.J., Grabowski, W.W., Guichard, F., Johnson, D.E., Khairoutdinov, M., Krueger, S.K., Petch, J.C., Randall, D.A., Seman, C.J., Tao, W.-K., Wang, D., Xie, S.C., Yio, J.J., Zhang, M.-H., 2002. An intercomparison of cloud-resolving models with the Atmospheric Radiation Measurement summer 1997 Intensive Observation Period data. Q. J. R. Meteor. Soc. 128, 593–624.
Yanai, M., Esbensen, S., Chu, J., 1973. Determination of bulk properties of tropical cloud clusters from large-scale heat and moisture budgets. J. Atmos. Sci. 30, 611–627.
Zhang, G.J., McFarlane, N.A., 1995. Sensitivity of climate simulations to the parameterization of cumulus convection in the Canadian Climate Center general circulation model. Atmos.-ocean. 33, 407–446.

Akio Arakawa, a professor emeritus, has been a faculty of the department of atmospheric and oceanic sciences at UCLA for 46 years. Born in Japan, he received his D.Sc. in meteorology from the University of Tokyo. He has made significant contributions in the area of atmospheric dynamics and modeling, especially in the development of the numerical methods that permit long-term integrations and the way representing convective clouds in atmospheric models that do not explicitly resolve them. He is the recipient of Carl-Gustaf Rossby Research Medal (AMS, 1977) and Vilhelm Bjerknes Medal (EGU, 2010).

Joon-Hee Jung, a research scientist, has been with the department of atmospheric science at Colorado State University for 7 years. She received a PhD in meteorology from Yonsei University, Korea. Prior to her current position, she worked at UCLA as a postdoctoral research fellow with professors Akio Arakawa and Carlos R. Mechoso. As one of the main contributors to a project on multi-scale modeling of atmospheric processes, she has been working on the conceptual and technical design of the new modeling framework that unifies different scales of motions and physical processes.